A NOVEL IMPLEMENTATION OF AXISYMMETRICALLY ORTHOTROPIC
MATERIAL MODEL TO LONGITUDINALLY CUT WOOD-LIKE THICK PLATES
FOR EXAMINING THE FREQUENCY BEHAVIOR USING FEM


by
Ahmet  Kerem Leblebici


Submitted to the Institute of Graduate Studies in
Science and Engineering in partial fulfillment of
the requirements for the degree of
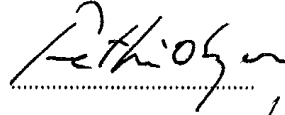Master of Science
in
Mechanical Engineering
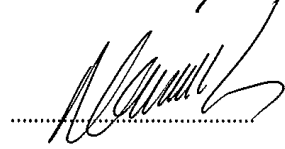

Yeditepe University
2011

A NOVEL IMPLEMENTATION OF AXISYMMETRICALLY ORTHOTROPIC
MATERIAL MODEL TO LONGITUDINALLY CUT WOOD-LIKE THICK PLATES
FOR EXAMINING THE FREQUENCY BEHAVIOR USING FEM

APPROVED BY:

Assist. Prof. Fethi Okyar
(Supervisor)

Assist. Prof. Namık Çıblak
(Co-Supervisor)

Prof. Dr. Cengiz Toklu

DATE OF APPROVAL: 01/08/2011

# ACKNOWLEDGEMENTS

# ABSTRACT

## A NOVEL IMPLEMENTATION OF AXISYMMETRICALLY ORTHOTROPIC MATERIAL MODEL TO LONGITUDINALLY CUT WOOD-LIKE THICK PLATES FOR EXAMINING THE FREQUENCY BEHAVIOR USING FEM

Wood is usually modeled as a classical orthotropic material. In actuality, the principal axes of orthotropy are dependent on the location. In fact, the principal axes are aligned with the cylindrical axes of the annual rings that form the trunk from which the wood is cut. These axes are conventionally named as longitudinal (L), radial (R), and tangential (T). There exist numerious papers that studied the vibrational characterictics, such as resonance and mode shapes, of the plates with different boundary conditions. To the best of our knowledge, all of these studies used either isotropic or classically orthotropic material behavior in the analyses. In this study, a new plate type finite element is developed that takes into account the variation in the alignment of the principal axes of orthotropy, and a number of analyses are performed using this developed model.

# ÖZET

# AĞAÇ VE BENZERİ YAPIDAKİ BOYLAMSAL OLARAK KESİLMİŞ İNCE PLAKALARIN SONLU ELEMANLAR METODU KULLANILARAK FREKANS DAVRANIŞLARININ İNCELENMESİNDE AKSİSİMETRİK ORTOTROPİK MALZEME MODELİNİN KULLANIMININ YENİ BİR UYGULAMASI

Ağaç genellikle klasik ortotropik malzeme olarak modellenmektedir. Gerçekte ortotropinin esas eksenleri konuma bağlı olarak değişmektedir. Gerçekte bu esas eksenler ağacın gövdesini oluşturan yıllık halkaların silindirik eksenleriyle hizalanmış durumdadır. Bu eksenler geleneksel olarak boylamsal, radyal ve teğetsel diye adlandırılır. Rezonans ve mod şekli gibi titreşim karakteristiklerinin çalışıldığı çok sayıda makale bulunmaktadır. Bilindiği kadarıyla bu mevcut çalışmaların tamamı analizlerinde izotropik ya da klasik ortotropik malzeme modellerinden birini kullanmaktadır. Bu çalışmamızda ortotropinin esas eksenlerinin konumlanmasındaki varyasyonu dikkate alacak şekilde yeni bir sonlu elemanlar element tipi geliştirilmiştir ve bu model kullanılarak birçok farklı analiz gerçekleştirilmiştir.

# TABLE OF CONTENTS

## LIST OF FIGURES

# LIST OF TABLES

# LIST OF SYMBOLS/ABBREVIATIONS

| | |
|---|---|
| a | Radial offset |
| AOMM | Axisymmetrically orthotropic material model |
| C | Compliance matrix |
| $\boldsymbol{D}$ | Reduced stiffness matrix's normal stress-strain part |
| $\boldsymbol{DM}$ | Diagonal matrix |
| dmg | Finite element representation of $\boldsymbol{D}$ |
| $dsg$ | Finite element representation of $\boldsymbol{\alpha}$ |
| F | Flexural rigidity |
| FEAP | Name of the finite element solver |
| G | Shear moduli |
| h | Thickness |
| $\mathbf{H}$ | Mass matrix |
| I | Inertia |
| $I_0$ | Principal inertia |
| $I_2$ | Rotator inertia |
| K | Component of reduced stiffness matrix's normal stress-strain part |
| $\mathbf{K_G}$ | Geometric stiffness matrix |
| $\mathbf{K_T}$ | Tangent stiffness matrix |
| L | Longitudinal axis |
| $\mathbf{M}$ | Tangential offset |
| m | Nodal circle |
| n | Nodal diameter |

| | |
|---|---|
| $q_0$ | Distributed transverse loading |
| R | Radial axis |
| r | Radial position |
| S | Stiffness matrix |
| s | Tangential offset |
| **S** | Shear force resultants matrix |
| T | Tangential axis |
| **T** | Transformation matrix |
| *u* | Displacement in x-direction |
| U | Strain energy |
| **UT** | Upper triangular matrix |
| *v* | Displacement in y-direction |
| w | Displacement in z-direction |
| *W* | Strain energy density per unit volume |
| **X** | Eigenvector |
| | |
| **α** | Reduced stiffness matrix including the shear terms |
| $\gamma$ | Shear strain |
| $\varepsilon$ | Strain tensor |
| $\theta$ | Orthotropic orientation angle |
| $\lambda$ | Eigenvalue |
| $\nu$ | Poisson's ratio |
| $\Pi_{bt}$ | Boundary terms |
| $\rho$ | Mass density |

| | |
|---|---|
| $\sigma$ | Stress tensor |
| $\tau$ | Shear stress |
| $\omega$ | Natural frequency |

# 1. INTRODUCTION

Orthotropic plates are commonly used in many fields of structural engineering such as aerospace, ocean structures, mechanical, and naval [1]. There are numerous types of solutions for the vibration of the orthotropic rectangular plates in the literature. One of the earliest studies about the fundamental frequency of vibration of orthotropic plates is done by Hearmon [2]. He defined the most fundamental differential equations governing the vibration of plates, and derived the frequency equations for the plates clamped at egdes and simply supported at edges. The derivations of fundamental frequency were done using the Rayleigh method where the maximum potential energy of bending is assumed as equal to the maximum kinetic energy, and the frequency of vibration results are found from this equality. The boundary condition definitions are given by Timoshenko in [3]. Leissa [4] also applied Rayleigh and Rayleigh-Ritz methods of analysis to obtain the natural frequencies with the use of beam characteristic functions. In another one of Liessa's works [5] studied free vibrations of rectangular plates for several isotropic cases and boundary conditions. Hearmon [6] improved Warburton's study [7] for specially orthotropic plates with any of its edges either clamped or supported. Jones and Milne [8] analysed the transverse vibrations of rectangular plates by using the extended Kantorovich method which is a Galerkin-based averaging technique. The closed form solution is obtained for several combinations of boundary conditions. Bhat [9] obtained the natural frequency response of rectangular plates by employing a set of beam characteristic orthogonal polynomials in Rayleigh-Ritz method. Gram-Schmidt process is used to generate the orthogonal polynomials, and once the natural frequencies are obtained using the orthogonal polynomial functions, the results are compared with the previous studies. Sakata et al. [10] obtained the natural frequencies of rectangular plates by successive reduction of the governing partial differential equation. They assumed an approximate solution satisfying the boundary conditions along one direction and employing the Kantorovich method. Kim [11] used Rayleigh-Ritz method with products of simple polynomials as the admissable functions. The study analyzed the natural frequencies of orthotropic, elliptical and circular plates with free, simply supported, and clamped boundary conditions. Convergence tests were conducted for different geometrical aspect ratios, and the lowest three frequency-

related parameters were compared. Biancolini [12] defined a new quick approximate method using a particular formulation of the Rayleigh method for the solution of free vibrations of thin orthotropic rectangular plates at various boundary conditions. The method was base on the assumption that the deformed shape *w(x,y)* is equal to the superposition of *wi(x,y)* due to fundamental frequency of each part. However, this method is useless for the isotropic plates with complex shapes of nodal lines. Rossi, who was one of the scientists that studied the subject numerically, defined a finite element procedure to compare analytical and numerical solutions of vibrations of a rectangular orthotropic plate with a free edges [13].

On the other hand, there are also some studies of frequencies of orthotropic plates with varying thickness in literature. Generally, the aims of designing a plate with tapered thickness are, 1) to alter the resonant frequency, and 2) to reduce the weight and size of the structures. Sakata [14] derived the characteristic equation of a clamped orthotropic rectangular plate with varying thickness in one direction parallel to the side, by the use of a double trigonometric solution. In the same study,  the influence of flexural rigidities on the natural frequency responses for both isotropic and orthotropic cases were illustrated. A new set of beam functions using with the Rayleigh-Ritz method were developed by Cheung [15], and the free vibrations of linearly tapered and parabotically tapered rectangular plates for different boundary conditions were analysed in different directions using various taper factors. Grigorenko and Tregubenko [16] made a comparison of the dimensionless fundamental frequency of rectangular plates with variable thicknesses using different methods such as Rayleigh-Ritz's method, Edmann's method, and Bolotin's method. They also developed an alternative analytical solution to the problem using the Kirchhoff-Love theory. Huang et al. [17] applied the Green's function to establish the characteristic equation of free vibration of non-uniform rectangular orthotropic plates. They transformed the differential equations into integral equations by taking into consideration the boundary conditions, aspect ratios, and the variation of the thickness. They used variables thicknesses in one and two directions, and gave the natural frequency responses for different boundary conditions, and different mode sequence numbers. There are also some studies for natural frequencies of circular plates with non-uniform thickness. Studies of Dian-Yun Chen et al.[18], and Chakraverty [19] et al. are the examples of such

analyses. This should also be noted here that there are not as much studies of natural frequencies of circular plates in the literature as rectangular plates.

The studies mentioned above are related with the frequency response of plates made of isotropic or orthotropic materials. Now, some further studies of orthotropic plates, specifically made of wood (an axisymmetrically-orthotropic composite material found in nature) will be mentioned. Hearmon [2], was found to be one of the pioneers in this field, who used the Rayleigh and Ritz methods to derive expressions leading to natural frequencies of orthotropic plates made of wood. However, the axisymmetric nature of wood's orthotropy was neglected. He also conducted experiments on wood and plywood plates to determine orthotropic elasticity parameters, and compare frequencies of vibration between the numerical results and experimental ones. Goodman et al. [20] provided a monumental experimental study, with nearly 900 experiments on wood samples made of differents types of logs, cut at various grain and ring angles. They obtained the orthotropic elastic parameters of four different anatomical families of trees. The effective modulus variation with respect to grain and ring angles were provided in their study, both theoretically and experimentally. Mascia et al. [21] listed some remarks about orthotropic elastic models applied to wood. They listed some previous studies about the effect of grain angles of wood, macroscopic structure of wood, and gave some theoretical and experimental examples. Noack et al. [22] determined the fundamental equations concerning the second boundary value problem of theory of elasticity for construction wood assuming the plain stress condition. Lawrence et al. [23] compared elastic constants that were obtained by mechanical testing with those found by ultrasonic wave propagation method.

Many studies mentioned above are about the experimental determination of material parameters of wood which is not a trivial procedure due to the nonhomogeneous nature of wood's microstructure. Wood does not exhibit material symmetry as understood in the conventional sense-where the principal directions of orthotropy are spatially invariant-, especially when it is cut in the form of plates. This has been an ongoing concern in the previous studies, as stated in [20] and [21]. Because of the axisymmetric nature of its grain structure, the principal directions of orthotropy varies continuously as a function of

spatial coordinates. Therefore, the idealized orthotropic elastic behavior may not be as suitable for wood as previous studies have hoped for, in characterizing its mechanical and vibrational behavior. The variation in the principal orthotropic directions of wood, is chiefly due to the ring curvature and also possibly to the spirally grained structure as indicated in [20]. As noted in Goodman's study, small deviations in grains can produce large changes in the stiffness matrix of wood.

In this study, we aimed at developing a concise formulation that takes into account the aforementioned axisymmetric nature of orthotropy, exhibited by wood. The formulation is especially suitable for finite elements analysis of the frequency response of wooden plates, that were cut longitudinally from logs. The distance between the plane of cut and the longitudinal axis of the log - which is used to calculate the ring curvature-, is the main parameter for the determination of a pointwise stiffness matrix. An existing quadrilateral plate-type finite element subroutine was modified, and the calculation of stiffness matrix was re-defined. The new element type was tested under a set of conditions.

# 2. THEORY

## 2.1. CONSTITUTIVE BEHAVIOR

### 2.1.1. Anisotropy, Orthotropy and Isotropy

The relationship between the strain and the applied stress is commonly used to characterize a material. These stress-strain relationships for linear materials are known as Hooke's law. In most general form of Hooke's law 81 material constants are required. Symmetry in the stress and strain tensors reduces this number to 36 elastic constants. The matrix is symmetric which reduces the number of elastic constants to 21. The 21 material constants can be reduced to 9 for a cylindrical system if symmetry exists in the material.

In general, each stress component is a function of all strain components. The generalized Hooke's law relating stresses to strains can be written in contracted notation as

$$\sigma_i = S_{ij}\varepsilon_j \tag{2.1}$$

where $\sigma_i$ are the components of the stress tensor, $S_{ij}$ is the stiffness matrix, and $\varepsilon_j$ are the components of strain tensor for i, j = 1, 2, ..., 6. In writing Eqn.(2.1), the summation convention is implied over the repeating indices. The contracted notation is defined in comparison to the usual tensor notation for three-dimensional strains and stresses for situations in which the stress and strain tensors are symmetric. Therefore in contracted notation, the strains are

$$\varepsilon_1 = \varepsilon_x = \frac{\partial u}{\partial x} \tag{2.2}$$

$$\varepsilon_2 = \varepsilon_y = \frac{\partial v}{\partial y} \tag{2.3}$$

$$\varepsilon_3 = \varepsilon_z = \frac{\partial w}{\partial z} \tag{2.4}$$

$$\varepsilon_4 = \gamma_{yz} = \frac{\partial v}{\partial z} + \frac{\partial w}{\partial y} \tag{2.5}$$

$$\varepsilon_5 = \gamma_{zx} = \frac{\partial w}{\partial x} + \frac{\partial u}{\partial z} \tag{2.6}$$

$$\varepsilon_6 = \gamma_{xy} = \frac{\partial u}{\partial y} + \frac{\partial v}{\partial x} \tag{2.7}$$

where *u*, *v*, and *w* are displacements in the *x*, *y*, and *z* directions [24].

The stiffness matrix, $S_{ij}$, in Eqn. (2.1) has 36 constants. Hovewer, only some of these are independent for elastic materials, when the strain energy is considered. For elastic materials the strain energy density per unit volume is defined as

$$dU = \sigma_i d\varepsilon_i \tag{2.8}$$

where the stress $\sigma_i$ acts through an infinitesimal strain $d\varepsilon_i$. Substituting for $\sigma_i$ from Eqn. (2.1) we get

$$dU = S_{ij}\varepsilon_j d\varepsilon_i \tag{2.9}$$

Upon integration, the strain energy density per unit of volume becomes

$$W = \frac{1}{2} S_{ij} \varepsilon_i \varepsilon_j \tag{2.10}$$

Note that the Hooke's law in Eqn. (2.1) can be derived from Eqn (2.11) by differentiating the strain energy density with respect to the strain components as

$$\frac{\partial W}{\partial \varepsilon_i} = S_{ij} \varepsilon_j \tag{2.11}$$

Differentiating this equation once more with respect to the $\varepsilon_j$, we get:

$$\frac{\partial^2 W}{\partial \varepsilon_i \partial \varepsilon_j} = S_{ij} \tag{2.12}$$

which implies the symmetry $S_{ij} = S_{ij}$ since the order of differentation of W is immaterial.

From the symmetry consideration of $S_{ij}$ shown above, the stiffness matrix has only 21 independent constants. In similar manner, the compliance matrix $C_{ij}$ which gives the strain in terms of stresses as

$$\varepsilon_i = C_{ij} \sigma_j \tag{2.13}$$

for i, j = 1, 2, ....., 6 can be shown to be symmetric based on the same consideration above.

With the reduction operation from 36 to 21 independent constants, the stress-strain relation (in Voigt notation) becomes

$$\begin{pmatrix} \sigma_1 \\ \sigma_2 \\ \sigma_3 \\ \sigma_4 \\ \sigma_5 \\ \sigma_6 \end{pmatrix} = \begin{bmatrix} S_{11} & S_{12} & S_{13} & S_{14} & S_{15} & S_{16} \\ S_{12} & S_{22} & S_{23} & S_{24} & S_{25} & S_{26} \\ S_{13} & S_{23} & S_{33} & S_{34} & S_{35} & S_{36} \\ S_{14} & S_{24} & S_{34} & S_{44} & S_{45} & S_{46} \\ S_{15} & S_{25} & S_{35} & S_{45} & S_{55} & S_{56} \\ S_{16} & S_{26} & S_{36} & S_{46} & S_{56} & S_{66} \end{bmatrix} \begin{pmatrix} \varepsilon_1 \\ \varepsilon_2 \\ \varepsilon_3 \\ \varepsilon_4 \\ \varepsilon_5 \\ \varepsilon_6 \end{pmatrix} \tag{2.14}$$

where $\sigma_1 = \sigma_x$, $\sigma_2 = \sigma_y$, $\sigma_3 = \sigma_z$, $\sigma_4 = \tau_{yz}$, $\sigma_5 = \tau_{zx}$, $\sigma_6 = \tau_{xy}$, $\varepsilon_1 = \varepsilon_x$, $\varepsilon_2 = \varepsilon_y$, $\varepsilon_3 = \varepsilon_z$, $\varepsilon_4 = 2\varepsilon_{yz}$, $\varepsilon_5 = 2\varepsilon_{zx}$, $\varepsilon_6 = 2\varepsilon_{xy}$.

This is the most general expression defining the stress-strain relationship within the framework of linear elasticity. The Eqn (2.14) is referred to as characterizing an anisotropic material which does not take into account any planes of symmetry in material properties.

When a symmetry plane in regard to the properties of a material brings certain restrictions as far as the components of the stiffness matrix involved. When a single plane of material property symmetry exists, the stress-strain relations reduce to the form:

$$
\begin{pmatrix} \sigma_1 \\ \sigma_2 \\ \sigma_3 \\ \sigma_4 \\ \sigma_5 \\ \sigma_6 \end{pmatrix}
=
\begin{bmatrix}
S_{11} & S_{12} & S_{13} & 0 & 0 & S_{16} \\
S_{12} & S_{22} & S_{23} & 0 & 0 & S_{26} \\
S_{13} & S_{23} & S_{33} & 0 & 0 & S_{36} \\
0 & 0 & 0 & S_{44} & S_{45} & 0 \\
0 & 0 & 0 & S_{45} & S_{55} & 0 \\
S_{16} & S_{26} & S_{36} & 0 & 0 & S_{66}
\end{bmatrix}
\begin{pmatrix} \varepsilon_1 \\ \varepsilon_2 \\ \varepsilon_3 \\ \varepsilon_4 \\ \varepsilon_5 \\ \varepsilon_6 \end{pmatrix}
\tag{2.15}
$$

where the symmetry plane is $z = 0$. Such a material is called a monoclinic material which has 13 independent elastic constants.

If a material possesses symmetry with respect to two orthogonal planes, then it is necessarily true that symmetry conditions also prevail in the third mutually orthogonal plane [25]. In that case, the relation expressed in a system of Cartesian coordinates aligned with the principal material directions is

$$
\begin{pmatrix} \sigma_1 \\ \sigma_2 \\ \sigma_3 \\ \sigma_4 \\ \sigma_5 \\ \sigma_6 \end{pmatrix}
=
\begin{bmatrix}
S_{11} & S_{12} & S_{13} & 0 & 0 & 0 \\
S_{12} & S_{22} & S_{23} & 0 & 0 & 0 \\
S_{13} & S_{23} & S_{33} & 0 & 0 & 0 \\
0 & 0 & 0 & S_{44} & 0 & 0 \\
0 & 0 & 0 & 0 & S_{55} & 0 \\
0 & 0 & 0 & 0 & 0 & S_{66}
\end{bmatrix}
\begin{pmatrix} \varepsilon_1 \\ \varepsilon_2 \\ \varepsilon_3 \\ \varepsilon_4 \\ \varepsilon_5 \\ \varepsilon_6 \end{pmatrix}
\tag{2.16}
$$

where

$$S_{11} = \frac{1 - v_{23}v_{32}}{\Delta} * E_1 \qquad (2.17)$$

$$S_{12} = \frac{v_{12} + v_{31}v_{23}}{\Delta} * E_1 = \frac{v_{12} + v_{32}v_{13}}{\Delta} * E_2 \qquad (2.18)$$

$$S_{13} = \frac{v_{31} + v_{21}v_{32}}{\Delta} * E_1 = \frac{v_{13} + v_{12}v_{23}}{\Delta} * E_3 \qquad (2.19)$$

$$S_{22} = \frac{1 - v_{13}v_{31}}{\Delta} * E_2 \qquad (2.20)$$

$$S_{23} = \frac{v_{32} + v_{12}v_{31}}{\Delta} * E_2 = \frac{v_{23} + v_{21}v_{13}}{\Delta} * E_3 \qquad (2.21)$$

$$S_{33} = \frac{1 - v_{12}v_{21}}{\Delta} * E_3 \qquad (2.22)$$

$$S_{44} = S_{23} \qquad (2.23)$$

$$S_{55} = S_{31} \qquad (2.24)$$

$$S_{66} = S_{12} \qquad (2.25)$$

$$\Delta = 1 - v_{12}v_{21} - v_{23}v_{32} - v_{31}v_{13} - 2*v_{21}v_{32}v_{13} \qquad (2.26)$$

Here, $E_1$, $E_2$ and $E_3$ are the Young's moduli in principal material directions, and $G_{23}$, $G_{31}$, and $G_{12}$ are shear moduli values in the principal material planes associated with these directions. Finally, $v_{ij}$ is the Poisson's ratio for transverse strain in the *j*-direction when stressed in the *i*-direction (i.e. $v_{ij} = - \varepsilon_j / \varepsilon_i$).

This type of a constitutive relation completes the description of the orthotropic behavior in a material. In this case, there is no interaction between normal stresses and shearing strains contrary to anisotropic materials. In addition, there is no interaction between sheraing stresses and normal strains as well as none between shearing stresses and shearing strains in different planes. For an orthotropic material, there are only nine independent constants in the stiffness matrix.

When the material properties exhibit no dependence to the orientation along which they are tested, they are said to have an infinite number of planes of material property symmetry, and the relations simplify to that of an isotropic material which has only two independent constants in the stiffness matrix. The related matrix is shown below:

$$
\begin{pmatrix} \sigma_1 \\ \sigma_2 \\ \sigma_3 \\ \sigma_4 \\ \sigma_5 \\ \sigma_6 \end{pmatrix} = \begin{bmatrix} S_{11} & S_{12} & S_{12} & 0 & 0 & 0 \\ S_{12} & S_{11} & S_{12} & 0 & 0 & 0 \\ S_{12} & S_{12} & S_{11} & 0 & 0 & 0 \\ 0 & 0 & 0 & (S_{11} - S_{12})/2 & 0 & 0 \\ 0 & 0 & 0 & 0 & (S_{11} - S_{12})/2 & 0 \\ 0 & 0 & 0 & 0 & 0 & (S_{11} - S_{12})/2 \end{bmatrix} \begin{pmatrix} \varepsilon_1 \\ \varepsilon_2 \\ \varepsilon_3 \\ \varepsilon_4 \\ \varepsilon_5 \\ \varepsilon_6 \end{pmatrix} \quad (2.27)
$$

## 2.1.2. Orthotropy in Wood

Wood is known to be one of the most common types of orthotropic materials found in nature. It has unique and independent mechanical properties in the directions of three mutually perpendicular axes: Longitudinal (1), tangential (2) and radial (3). The longitudinal axis L is parallel to fiber (grain); the radial axis R is normal to the growth rings (perpendicular to the grain in the radial direction); and the tangential axis T is perpendicular to the grain but tangent to the growth rings. These axes are shown in Figure 2.1. The mechanical properties of wood in the radial direction are much higher than those

in the tangential direction. In addition, both radial and tangential properties are about one order of magnitude lower than the properties in the longitudinal direction [28]. The difference between the mechanical properties of wood in tangential and radial directions is explained by the cell shape in the cross-section plane causing the anisotropy in the transverse plane [29] and/or by the effect of rays in the radial direction [30]. In addition, wood's fracture toughness is very high compared with relative weakness of its constituents. The fracture toughness of the wood is also affected by its microstructure. So, it is observed that the toughness in the TR direction is higher than that in the TL direction [31]. There are also some other characteristics that make wood different from composites: effect of moisture which leads to decrease of the strength of wood, dimensional instability which can be seen as a result of the moisture effect, time-dependent deformation which is a result of the movement of the non-crystalline (amorphous) sections of the cellulose microfibrils, large variability in properties among the species of the wood [32].

Interestingly, due to the natural formation of the growth of trees, a wooden log exhibits a unique orthotropic behavior. In the theory of elasticity, wood is described as an orthotropic body with a cylindrical anisotropy [26], which is why we call it as an axisymmetrically orthotropic material. An axisymmetrically orthotropic material is one whose principal directions are defined in a cylindrical coordinate system. Its properties remain invariant with respect to coordinates. However, in Cartesian coordinates, the principal material directions vary as a function of position, that is the invariance property is lost.
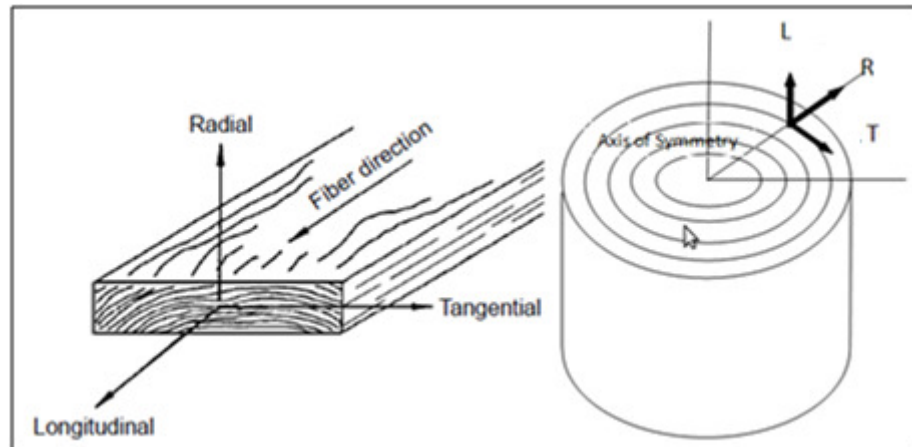
Figure 2.1. Principal directions of wood (Illustration is taken from [27])

Clear wood (clear wood specimens are considered as "homogeneous" in wood mechanics) is commonly assumed to obey the linear elastic orthotropic material law locally. That means, if Cartesian coordiantes are used to express the mechanics of deformation, the homogeniety is only valid in a local base due to its ringed structure and the fact that its principal axes rotate from point to point. However, if a cylindrical coordinate system is used instead, its properties become invariant of location, provided that the rings are assumed to be ideally circular and they extend perpendicularly from its base.

From Figure 2.2, this can be seen that for a longitudinally cut plate orthotropic orientation varies as a function of radial position. As the radial distance changes from point A to point B, the angle that specifies the orthotropic orientation changes from $\theta_A$ to $\theta_B$. Then the elasticity tensor is also expected to change from point A to point B.
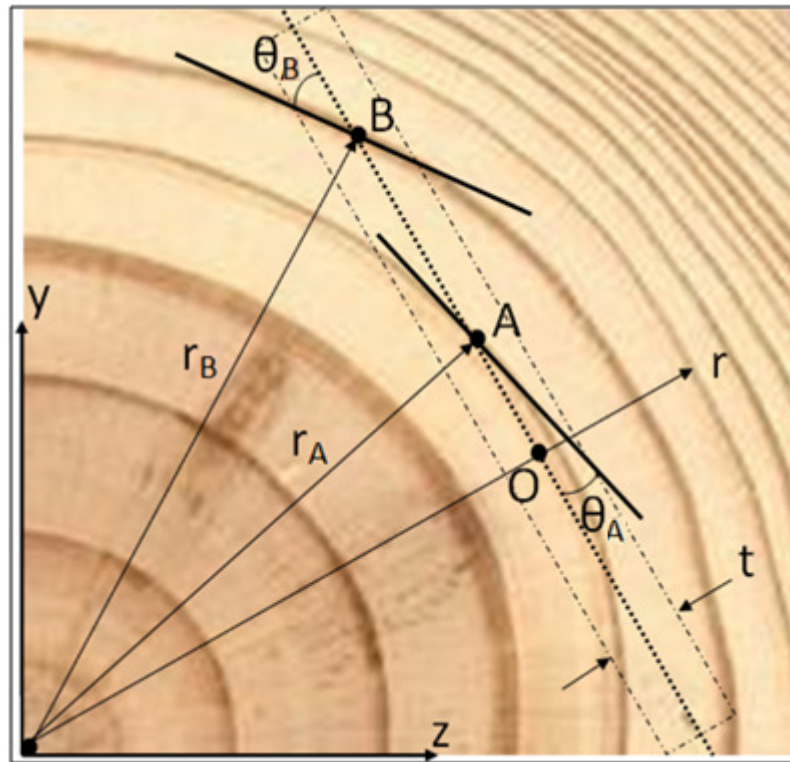
Figure 2.2. Variation of the orthotropic orientation angle as moving through a point to another one on the longitudinally cut wood log

As a result to fully understand the elastic mechanical properties of wood (how it bends and deforms elastically), one needs 12 elastic properties: 3 moduli of elasticity (one for each direction), 3 moduli of rigidity (one for each direction), and 6 Poisson's ratios (only three of them are independent). The moduli of elasticity are parameters that define how "stiff" or elastic a material is. The modulus of rigidity is similar but is more often used to characterize how "stiff" a material is when it is twisted or put into a state of torsion. Poisson's ratio defines how a material deforms when stressed. The general orthotropic material behavior for wood is given in the principal directions is given at Eqn. (2.28). From that point, the procedures for formation of the stiffness matrix of orthotropy in wood are mostly taken from Cıblak's unpublished manuscript [33].

$$\begin{pmatrix} \varepsilon_L \\ \varepsilon_T \\ \varepsilon_R \\ \varepsilon_{TR} \\ \varepsilon_{RL} \\ \varepsilon_{LT} \end{pmatrix} = \begin{bmatrix} 1/E_L & -\nu_{TL}/E_T & -\nu_{RL}/E_R & 0 & 0 & 0 \\ -\nu_{LT}/E_L & 1/E_T & -\nu_{RT}/E_R & 0 & 0 & 0 \\ -\nu_{LR}/E_L & -\nu_{TR}/E_T & 1/E_R & 0 & 0 & 0 \\ 0 & 0 & 0 & 1/2*G_{TR} & 0 & 0 \\ 0 & 0 & 0 & 0 & 1/2*G_{RL} & 0 \\ 0 & 0 & 0 & 0 & 0 & 1/2*G_{LT} \end{bmatrix} \begin{pmatrix} \sigma_L \\ \sigma_T \\ \sigma_R \\ \sigma_{TR} \\ \sigma_{RL} \\ \sigma_{LT} \end{pmatrix} \quad (2.28)$$

where $\sigma_L=\sigma_1$, $\sigma_T=\sigma_2$, $\sigma_R=\sigma_3$, $\sigma_{TR}=\tau_4$, $\sigma_{RL}=\tau_5$, $\sigma_{LT}=\tau_6$, $\varepsilon_L= \varepsilon_1$, $\varepsilon_T= \varepsilon_2$, $\varepsilon_R= \varepsilon_3$, $\varepsilon_{TR}= \varepsilon_4$, $\varepsilon_{RL}= \varepsilon_5$, $\varepsilon_{LT}= \varepsilon_6$

Here the single subscripts refer to the normal and double subscripts refer to shear components. The quantities subscripted by L, T, R are those along the longitudinal, radial and tangential axes of the wood.

For purposes of classical mechanics, the compliance matrix is required to be symmetric for a physically allowable material constitutive rule. Hence, the symmetry constraints can be written as follows:

$$\frac{\nu_{TL}}{E_T} = \frac{\nu_{LT}}{E_L} \quad (2.29)$$

$$\frac{\nu_{LR}}{E_L} = \frac{\nu_{RL}}{E_R} \quad (2.30)$$

$$\frac{\nu_{TR}}{E_T} = \frac{\nu_{RT}}{E_R} \quad (2.31)$$

This yields only nine independent material property constants, as is the case for general orthotropic material models.

For stiffness matrix representation the relationship between stress and strain is written as

$$[\sigma] = \tilde{S}[\varepsilon] \tag{2.32}$$

whose upper and lower 3 by 3 diagonal matrices are $S_{1\ldots3,1\ldots3}$

$$S_{1\ldots3,1\ldots3}= \frac{1}{\Delta} * \begin{bmatrix} (1-\nu_{RT}\nu_{TR})^*E_L & (\nu_{TL}+\nu_{TR}\nu_{RL})^*E_L & (\nu_{RL}+\nu_{RT}\nu_{TL})^*E_L \\ (\nu_{LT}+\nu_{LR}\nu_{RT})^*E_T & (1-\nu_{LR}\nu_{RL})^*E_T & (\nu_{RT}+\nu_{RL}\nu_{LT})^*E_T \\ (\nu_{LR}+\nu_{LT}\nu_{TR})^*E_R & (\nu_{TR}+\nu_{TL}\nu_{LR})^*E_R & (1-\nu_{TL}\nu_{LT})^*E_R \end{bmatrix}$$

$$S_{4\ldots6,4\ldots6}= \begin{bmatrix} G_{TR} & 0 & 0 \\ 0 & G_{RL} & 0 \\ 0 & 0 & G_{LT} \end{bmatrix} \tag{2.33}$$

where

$$\Delta=1 - \nu_{LT}\nu_{TL} - \nu_{TR}\nu_{RT} - \nu_{TR}\nu_{RT} - 2* \nu_{TL}\nu_{LR}\nu_{RT} \tag{2.34}$$

As one moves from point to point inside an axisyymetrically ortotropic material, the principal axes rotate, except for motions along L and R directions. Thus, for all thin plate cut-outs, except those whose xy-plane is formed by LR-axes, there is no classical homogenity. For the purposes of this study, only those cuts whose x-axes is aligned with the L-axis are considered, as shown in below Figure 2.3.
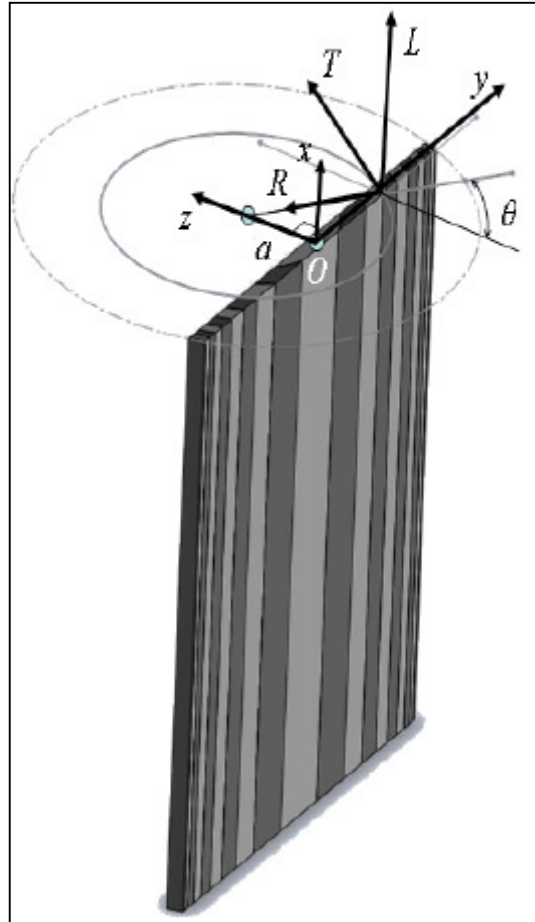
Figure 2.3. Longitudinally cut wood log showing the material coordinate system with scripts L, T, and R (Illustration is taken from [33])

From Figure 2.3, we can see that the R and L axes rotate with moving along the y-axis of the plate. The perpendicular distance from the center of the wood to mid-plane of the plate is denoted by a. The intersection point in the mid-plane is also selected as the origin O of the xyz system. The systems are chosen as right handed. As one travels along the +y direction, the principal axes rotate about the L-axis in positive sense. The angle of rotation is related to the position as follows:

$$\tan \theta = {}^y\!/_a \qquad (2.35)$$

Case a = 0 represents a cut through the center axis of the wood and the principal axes no longer rotates as one traverses the y-axis, however, the properties along the R and T directions are not distinguishable at the origin. Therefore, in the limit, the value of elastic modulus at radial axis becomes equal to elastic modulus at tangential axis. From now on, the formulation will be formed for the case that a value is different than zero.

To start with, the transformation matrix representation is given below:

$$T = \begin{bmatrix} 1 & 0 & 0 & 0 & 0 & 0 \\ 0 & \cos^2\theta & \sin^2\theta & -2\cos\theta\sin\theta & 0 & 0 \\ 0 & \sin^2\theta & \cos^2\theta & 2\cos\theta\sin\theta & 0 & 0 \\ 0 & \cos\theta\sin\theta & -\cos\theta\sin\theta & \cos^2\theta - \sin^2\theta & 0 & 0 \\ 0 & 0 & 0 & 0 & \cos\theta & \sin\theta \\ 0 & 0 & 0 & 0 & -\sin\theta & \cos\theta \end{bmatrix} \qquad (2.36)$$

Here, $\theta$ is the angle of rotation about the longitudinal axis, and it is measured positive according to the right hand rule.

In general, the stress and strain components transform using the tensor calculus according to

$$\overline{v_0} = \tilde{T}\bar{v} \qquad (2.37)$$

where $\overline{v_0}$ is the quantity at $\theta = 0$ and $\bar{v}$ is the quantity at $\theta = \theta^*$ which is an arbitrary angle. By using that transformation rule, the general stiffness and compliance matrices can be defined as

$$\tilde{S}_0 = \tilde{T}\tilde{S}\widetilde{T^{-1}} \qquad (2.38)$$

$$\widetilde{C_0} = \tilde{T}\tilde{C}\widetilde{T^{-1}} \qquad (2.39)$$

Since the engineering shear and strains are used in our study, the transformation eqauation for stiffness and compliance matrices should be written as

$$\widetilde{S_0} = \tilde{T}\tilde{S}\widetilde{T^T} \tag{2.40}$$

$$\widetilde{C_0} = \widetilde{T^{-T}}\tilde{C}\widetilde{T^{-1}} \tag{2.41}$$

Here, the relationsip between strain and stress can be written as below

$$[\varepsilon] = \widetilde{T^{-T}}\tilde{C}\widetilde{T^{-1}}[\sigma] \tag{2.42}$$

Here, for a thin plate assumption, only $\sigma_x$, $\sigma_y$, and $\sigma_{xy}$ are needed in moment equations. Thus the problem reduces to a more traceble form Therefore; only the following form is needed

$$\begin{bmatrix} \varepsilon_x \\ \varepsilon_y \\ 2\varepsilon_{xy} \end{bmatrix} = \begin{bmatrix} \cdots & \cdots & \cdots \\ \cdots & \cdots & \cdots \\ \cdots & \cdots & \cdots \end{bmatrix} \begin{bmatrix} \sigma_x \\ \sigma_y \\ \sigma_{xy} \end{bmatrix} \tag{2.43}$$

By inverting this matrix, one can obtain this equation

$$\begin{bmatrix} \sigma_x \\ \sigma_y \\ \sigma_{xy} \end{bmatrix} = \begin{bmatrix} K_{11} & K_{12} & 0 \\ K_{21} & K_{22} & 0 \\ 0 & 0 & K_{66} \end{bmatrix} \begin{bmatrix} \varepsilon_x \\ \varepsilon_y \\ 2\varepsilon_{xy} \end{bmatrix} \tag{2.44}$$

This coefficient matrix in the above equation is the reduced form of the stiffness matrix for a thin plate assumption. If one would like to obtain the shear terms from the stiffness matrix, the following open-form multiplication of matrices should be performed and appropriate 2 x 2 portion should be shown. For the matrix algebra multiplication process, L, T, and R are replaced with 1, 2, and 3, respectively as it is shown in Figure 2.1.

In open form, this equation can be written as below:

$$\widetilde{S}_0 = \widetilde{T}\widetilde{S}\widetilde{T}^T = \begin{bmatrix} 1 & 0 & 0 & 0 & 0 & 0 \\ 0 & \cos^2\theta & \sin^2\theta & -2\cos\theta\sin\theta & 0 & 0 \\ 0 & \sin^2\theta & \cos^2\theta & 2\cos\theta\sin\theta & 0 & 0 \\ 0 & \cos\theta\sin\theta & -\cos\theta\sin\theta & \cos^2\theta - \sin^2\theta & 0 & 0 \\ 0 & 0 & 0 & 0 & \cos\theta & \sin\theta \\ 0 & 0 & 0 & 0 & -\sin\theta & \cos\theta \end{bmatrix}$$

$$\frac{1}{\Delta} \begin{bmatrix} (1-v_{32}v_{23})*E_1 & (v_{21}+v_{23}v_{31})*E_1 & (v_{31}+v_{32}v_{21})*E_1 & 0 & 0 & 0 \\ (v_{12}+v_{13}v_{32})*E_2 & (1-v_{13}v_{31})*E_2 & (v_{32}+v_{31}v_{12})*E_2 & 0 & 0 & 0 \\ (v_{13}+v_{12}v_{23})*E_3 & (v_{23}+v_{21}v_{13})*E_3 & (1-v_{21}v_{12})*E_3 & 0 & 0 & 0 \\ 0 & 0 & 0 & \Delta G_{23} & 0 & 0 \\ 0 & 0 & 0 & 0 & \Delta G_{31} & 0 \\ 0 & 0 & 0 & 0 & 0 & \Delta G_{12} \end{bmatrix}$$

$$\begin{bmatrix} 1 & 0 & 0 & 0 & 0 & 0 \\ 0 & \cos^2\theta & \sin^2\theta & \cos\theta\sin\theta & 0 & 0 \\ 0 & \sin^2\theta & \cos^2\theta & -\cos\theta\sin\theta & 0 & 0 \\ 0 & -2\cos\theta\sin\theta & 2\cos\theta\sin\theta & \cos^2\theta - \sin^2\theta & 0 & 0 \\ 0 & 0 & 0 & 0 & \cos\theta & -\sin\theta \\ 0 & 0 & 0 & 0 & \sin\theta & \cos\theta \end{bmatrix}$$

$$= \begin{bmatrix} K_{11} & K_{12} & \dots & \dots & \dots & \dots \\ K_{21} & K_{22} & \dots & \dots & \dots & \dots \\ \dots & \dots & \dots & \dots & \dots & \dots \\ \dots & \dots & \dots & K_{44} & K_{45} & \dots \\ \dots & \dots & \dots & K_{54} & K_{55} & \dots \\ \dots & \dots & \dots & \dots & \dots & K_{66} \end{bmatrix} \qquad (2.45)$$

where $\Delta = 1 - v_{13}v_{31} - v_{23}v_{32} - v_{12}v_{31}v_{23} - v_{21}v_{13}v_{32} - v_{12}v_{21}$

Here the matrix can be divided into two portions: First 3 by 3 matrix, $D$, is the reduced form of the stiffness matrix for the normal and shear stresses, while the other 2 by 2 martix, $\alpha$, is for expressing the shear terms that are defined by the thick plate theory.

Here, $D$ is represented as

$$D = \begin{bmatrix} K_{11} & K_{12} & \dots \\ K_{21} & K_{22} & \dots \\ \dots & \dots & K_{66} \end{bmatrix} \qquad (2.46)$$

The calculation of the each term is given below for $D$ matrix.

$$K_{11} = \frac{1}{\Delta} \begin{bmatrix} 1 \\ 0 \\ 0 \\ 0 \\ 0 \\ 0 \end{bmatrix}^T \widetilde{S}_0 \begin{bmatrix} 1 \\ 0 \\ 0 \\ 0 \\ 0 \\ 0 \end{bmatrix} = \frac{E_1 - \nu_{23}\nu_{32}E_1}{\Delta} \tag{2.47}$$

$$K_{12} = \frac{1}{\Delta} \begin{bmatrix} 0 \\ 1 \\ 0 \\ 0 \\ 0 \\ 0 \end{bmatrix}^T \widetilde{S}_0 \begin{bmatrix} 1 \\ 0 \\ 0 \\ 0 \\ 0 \\ 0 \end{bmatrix} = \frac{E_2(\nu_{12} + \nu_{13}\nu_{32})\cos^2\theta + E_3(\nu_{13} + \nu_{12}\nu_{23})\sin^2\theta}{\Delta} \tag{2.48}$$

$$K_{12} = K_{21} \tag{2.49}$$

$$K_{22} = \frac{1}{\Delta} \begin{bmatrix} 0 \\ 1 \\ 0 \\ 0 \\ 0 \\ 0 \end{bmatrix}^T \widetilde{S}_0 \begin{bmatrix} 0 \\ 1 \\ 0 \\ 0 \\ 0 \\ 0 \end{bmatrix} \tag{2.50}$$

$$= \frac{E_2(1 - \nu_{13}\nu_{31})\cos^4\theta + E_3(1 - \nu_{12}\nu_{21})\sin^4\theta + (\sin^2\theta\cos^2\theta)(4\Delta G_{23} + \nu_{32}E_2 + \nu_{12}\nu_{31}E_2 + \nu_{21}\nu_{12}E_3 + \nu_{23}E_3)}{\Delta}$$

$$K_{66} = \frac{1}{\Delta} \begin{bmatrix} 0 \\ 0 \\ 0 \\ 0 \\ 0 \\ 1 \end{bmatrix}^T \widetilde{S}_0 \begin{bmatrix} 0 \\ 0 \\ 0 \\ 0 \\ 0 \\ 1 \end{bmatrix} = G_{12}\cos^2\theta + G_{31}\sin^2\theta \tag{2.51}$$

As the second part of the reduced stiffness matrix, $\alpha$, the $K_{44}$, $K_{55}$, $K_{45}$, and $K_{54}$ terms are the ones that include the shear terms (i.e. thick plate assumption method). This 2 by 2 matrix is given below:

$$\begin{bmatrix} \sigma_{TR} \\ \sigma_{RL} \end{bmatrix} = \begin{bmatrix} K_{44} & K_{45} \\ K_{54} & K_{55} \end{bmatrix} \begin{bmatrix} \varepsilon_{TR} \\ \varepsilon_{RL} \end{bmatrix} \quad \text{where} \quad \begin{bmatrix} K_{44} & K_{45} \\ K_{54} & K_{55} \end{bmatrix} = \alpha \tag{2.52}$$

where

$$\begin{aligned}
K_{44} &= \frac{1}{\Delta} \begin{bmatrix} 0 \\ 0 \\ 0 \\ 1 \\ 0 \\ 0 \end{bmatrix}^T \tilde{S}_0 \begin{bmatrix} 0 \\ 0 \\ 0 \\ 1 \\ 0 \\ 0 \end{bmatrix} \\
&= G_{23} \left( \cos^4 \theta + \sin^4 \theta \right) \\
&\quad + \sin^2 \theta \cos^2 \theta \left( \frac{E_2}{\Delta} (1 - \nu_{12}\nu_{21} - \nu_{21}\nu_{13} - \nu_{23}) \right. \\
&\quad + \frac{E_2}{\Delta} (1 - \nu_{12}\nu_{31} - \nu_{13}\nu_{31} - \nu_{32}) - 2G_{23}
\end{aligned} \tag{2.53}$$

$$K_{45} = \frac{1}{\Delta} \begin{bmatrix} 0 \\ 0 \\ 0 \\ 1 \\ 0 \\ 0 \end{bmatrix}^T \tilde{S}_0 \begin{bmatrix} 0 \\ 0 \\ 0 \\ 0 \\ 1 \\ 0 \end{bmatrix} = 0 \tag{2.54}$$

$$K_{54} = \frac{1}{\Delta} \begin{bmatrix} 0 \\ 0 \\ 0 \\ 0 \\ 1 \\ 0 \end{bmatrix}^T \tilde{S}_0 \begin{bmatrix} 0 \\ 0 \\ 0 \\ 1 \\ 0 \\ 0 \end{bmatrix} = 0 \tag{2.55}$$

$$K_{55} = \frac{1}{\Delta} \begin{bmatrix} 0 \\ 0 \\ 0 \\ 0 \\ 1 \\ 0 \end{bmatrix}^T \tilde{S}_0 \begin{bmatrix} 0 \\ 0 \\ 0 \\ 0 \\ 1 \\ 0 \end{bmatrix} = G_{31} \cos^2 \theta + G_{12} \sin^2 \theta \tag{2.56}$$

Thus, these operations complete the formation of stiffness matrix for axisymmetrically orthotropic material model applied for wood. These are adequate to make necessary changes in finite element material file. Details about the finite element code that we deal with are given at Appendix A. $\alpha$ and $D$ matrices are defined as *dsg* and *dmg* at this subroutine. This subroutine is a part of the plate element (plate2q.f) function defined at the finite element solver FEAP. Now, some limit cases will be examined in detail.

### 2.1.3. Limiting Cases

The general behavior of the stiffness matrix is defined at above part. However, the case of cutting the plate centrally, and the case of cutting the plate far away from the center of the wood should be examined mathematically as the limit cases of the operation. At the case of centrally cut plate where the radial offset parameter, $a$, becomes zero the term $\sin^2 \theta$ approaches one, and $\cos^2 \theta$ approaches zero. In this case, the stiffness terms simplify as below:

$$K_{11} = \frac{1}{1 - \nu_{31}\nu_{13}} E_L \qquad (2.57)$$

$$K_{12} = \frac{\nu_{13}}{1 - \nu_{31}\nu_{13}} E_3 \qquad (2.58)$$

$$K_{22} = \frac{1}{1 - \nu_{31}\nu_{13}} E_3 \qquad (2.59)$$

$$K_{66} = G_{31} \qquad (2.60)$$

In this case, the dependence to the position information (i.e. "y" information) of the stiffness coefficients is removed and the effect of material properties along the tangential axis becomes immaterial. For this location, the tangential properties' contributions disappear in the limit and only the radial and longitudinal remain in effect.

On the other hand, if the cutting plane is brought far away from the centroidal axis, i.e. as the radial offset approaches infinity, the terms $\sin^2\theta$ approaches zero, and $\cos^2\theta$ approaches one. In this case, the longitudinal and the tangential properties remain in effect while the contributions from the radial properties dissepear for the limit value. The stiffness matrix terms for this case are given below:

$$K_{11} = \frac{1}{1 - \nu_{21}\nu_{12}} E_1 \tag{2.61}$$

$$K_{12} = \frac{\nu_{12}}{1 - \nu_{21}\nu_{12}} E_2 \tag{2.62}$$

$$K_{22} = \frac{1}{1 - \nu_{21}\nu_{12}} E_2 \tag{2.63}$$

$$K_{66} = G_{12} \tag{2.64}$$

## 2.2. MECHANICS AND VIBRATION OF PLATES

A plate is a flat structural element with other dimensions much longer than its thickness and is subjected to loads that cause bending deformation and stretching. In most cases, the thickness of plate structures is about one-tenth or less of the smallest in-plane dimensions. When the thickness is one-twentieth of an in-plane dimension or less, they are called thin, otherwise they are said to be thick. Since our study is focused on the deflection and the frequency behavior of the plates for different kinds of boundary condition cases and for different geometrical shapes, the short theoretical information about these are mentioned at this part of the chapter. The mechanical and the vibration theory about the plates where we are interested with are explained, respectively.

## 2.2.1. Deformation at the Plates

The deformations at the plates are examined for different kinds of geometries. Every geometrical shape forms their own deformation formulas for different kinds of boundary conditions. For our studies purposes, the circular geometry case is selected to be formulized. To present the deformation analysis of the circle geometry for two different types of boundary conditions, the analytical analysis of the problem under uniformly distributed load $q_0$ which is given at [34] is examined.

For the analytical calculations, these formulas are used:

- For clamped case:

$$w(r) = \frac{q * a^4}{64 * D} * \left(1 - \frac{r^2}{a^2}\right)^2 \qquad (2.65)$$
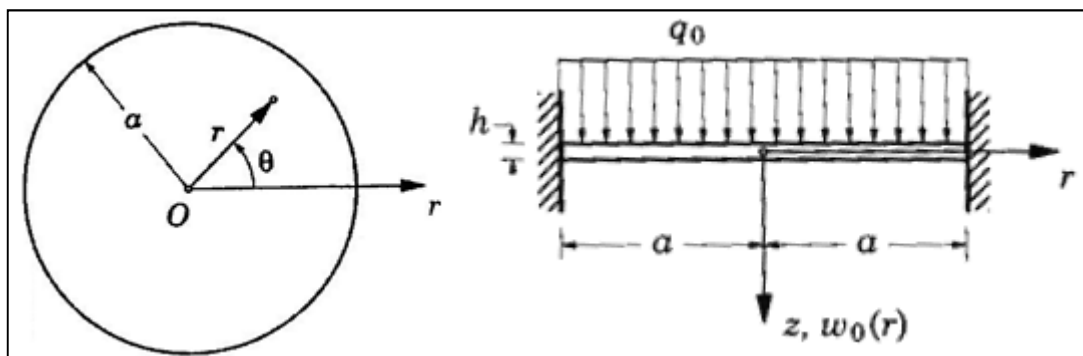


Figure 2.4. Clamped Circular Plate

- For simply supported case:

$$w(r) = \frac{q_0 * a^4}{64 * D} * [\left(\frac{r}{a}\right)^4 - 2 * \left(\frac{3+v}{1+v}\right) * \left(\frac{r}{a}\right)^2 + \left(\frac{5+v}{1+v}\right)] \qquad (2.66)$$
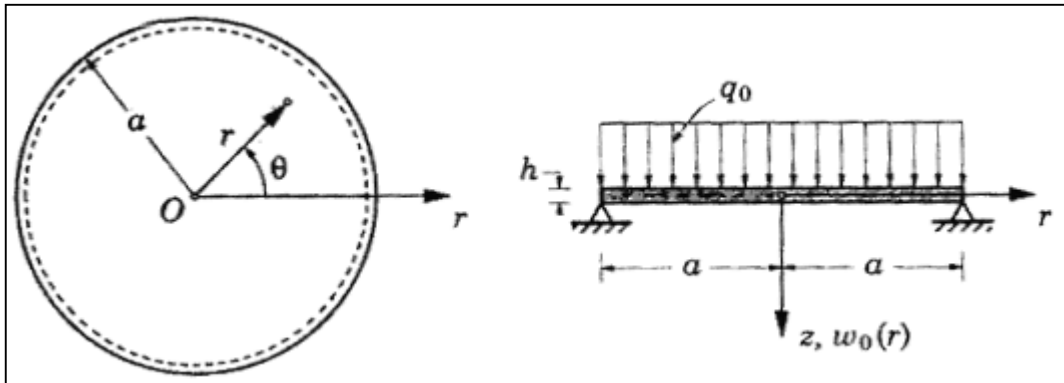
Figure 2.5. Simply Supported Circular Plate

In addition, the deflection of the cantilever beam at the tip formula is given at the below:
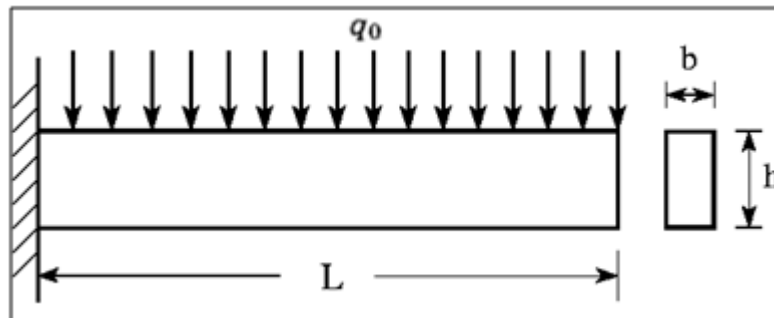


Figure 2.6. Cantilever Beam Geometry and the distributed loading onto the goemetry

The analytical deflection formula for the maximum deflection where the deflection takes place at the tip is given below:

$$w_{max} = \frac{q_0 * L^4}{8 * E_L * I} \tag{2.67}$$

where $I = (1/12)*b*h^3$.

## 2.2.2. Vibration at the Plates

The vibration analysis is an important part of the study, and to do that the solution of the eigenvalue-eigenvector problem for a multi degree of freedom system should be understand well.

The eigenvalues of an n by n matrix, $\mathbf{A}$, are the values of $\lambda$ such that the system of equations

$$\mathbf{A}\mathbf{x} = \lambda\,\mathbf{x} \tag{2.68}$$

has a nontrivial solution. An eigenvector is the nontrivial solution corresponding to an eigenvalue. The Eqn. (2.68) can be written as

$$(\mathbf{A} - \lambda\,\mathbf{I})\mathbf{x} = \mathbf{0} \tag{2.69}$$

where $\mathbf{x}$ is the n-dimensional column vector of generalized coordinates. From Cramer's Rule, the solution for $x_i$ is given as

$$x_i = \frac{0}{|\mathbf{A} - \lambda\,\mathbf{I}|} \tag{2.70}$$

Thus, for each i = 1,...., n, $x_i$ becomes zero, unless

$$|\mathbf{A} - \lambda\,\mathbf{I}| = 0 \tag{2.71}$$

The determinant of Eqn. (2.71) can be expanded by a column or row expansion. This yields an n-th order polynomial equation of the form

$$\lambda^{n} + C_1\lambda^{n-1} + C_1\lambda^{n-1} + \cdots + C_1\lambda^{n-1} + C_1\lambda^{n-1} = 0 \tag{2.72}$$

called the characteristic equation which has n roots, and $\mathbf{A}$ has n eigenvalues.

The reciprocals of the positive square roots of the eigenvalues of **AH** or the positive square roots of the eigenvalues **H**$^{-1}$**S** form the natural frequencies of an n-degree of freedom system. Here, **H** and **S** are the symmetric n by n mass matrix and stiffness matrix, respectively. All coefficients in the characteristic equation are real because all elements of the mass and stiffness matrices are real, and if complex roots are formed they should occur in complex conjugate pairs. The mode shape vectors are the corresponding eigenvectors and each distinct eigenvalue $\omega_i^2$, i = 1, 2,...., n, has a corresponding eigenvector, **X**$_i$, which satisfies

$$\boldsymbol{H}^{-1}\boldsymbol{S}\boldsymbol{X}_i = \omega_i^2 \boldsymbol{X}_i \qquad (2.73)$$

This mode shape, **X**$_i$, is an n-dimensional column vector, and it is shown in the form of

$$\boldsymbol{X}_i = \begin{bmatrix} X_{i1} \\ X_{i2} \\ ... \\ ... \\ X_{in} \end{bmatrix} \qquad (2.74)$$

The natural frequencies of a three-degree of freedom system can be obtained by finding the roots of a cubic polynomial, which are done by iterative method or trial and error way. The developement of a characteristic equation for an n-degree of freedom system requires the evaluation of an *n* by *n* determinant and the natural frequencies are called the *n* roots of the characteristic equation. The determinant of each of these eigenvector requires the solution of *n* algebraic equations. Thus for three or more number of degrees of freedom, the numerical methods which don't require the evaluation of the characteristic equation are used [35].

### 2.2.2.1. Free Vibrations

The free vibration concept is explained for two cases of application. For a clamped case application, a circular plate problem, which is given in the literature [36], is proceded

initially. Here, bending of a circular plate is considered. The equation of motion for this isotropic plate is given as:

$$F\nabla^2\nabla^2\omega_0 + k\omega_0 + I_0\frac{\partial^2\omega_0}{\partial t^2} - I_2\frac{\partial^2}{\partial t^2}(\nabla^2\omega_0) = 0 \qquad (2.75)$$

where $F$ is the flexural rigidity, $\nabla^2$ is the Laplace operator, $\omega_0$ is the transverse deflection, $k$ is the elastic foundation of modulus, $I_0\ (the\ principal\ inertia) = \rho h$, and $I_2\ (rotatory\ inertia) = \rho h^3/12$ where $h$ is the thickness. If free vibration is assumed, the deflection is periodic and it is expressed as

$$\omega_o(r,\theta,t) = W(r,\theta)\cos wt \qquad (2.76)$$

where $\omega$ is the circular frequency of vibration (radians per unit time), and W is a function of only r (radius) and $\theta$. Now, when the substitution of equation (2.76) into equation (2.75), the result is expressed as

$$F\nabla^2\nabla^2 W + kW - I_0\omega^2 W + I_2\omega^2\nabla^2 W = 0 \qquad (2.77)$$

The rotary inertia $I_2$ can be neglected from the Eqn. (2.77) since it contributes little to the frequencies. Thus, we get

$$(\nabla^4 - \beta^4)W = 0 \qquad (2.78)$$

where

$$\beta^4 = \frac{I_0\omega^2 - k}{D} \qquad (2.79)$$

Equation (2.78) can be factored into the form

$$(\nabla^2 + \beta^2)(\nabla^2 - \beta^2)W = 0 \tag{2.80}$$

so that the complete solution to Eqn. (2.80) is obtained by superimposing the solutions of the equations

$$(\nabla^2 W_1 + \beta^2 W_1) = 0, \qquad (\nabla^2 W_2 - \beta^2 W_2) = 0 \tag{2.81}$$

We now assume that the solution to equation (2.78) in the form of the general Fourier series as

$$W(r, \theta) = \sum_{n=0}^{\infty} W_n(r) \cos n\theta + \sum_{n=1}^{\infty} W_n^*(r) \sin n\theta \tag{2.82}$$

As the next step, subtitution of equation (2.82) into equation (2.81) yields

$$\frac{d^2 W_{n1}}{dr^2} + \frac{1}{r}\frac{dW_{n1}}{dr} - \left(\frac{n^2}{r^2} - \beta^2\right)W_{n1} = 0 \tag{2.83}$$

$$\frac{d^2 W_{n2}}{dr^2} + \frac{1}{r}\frac{dW_{n2}}{dr} - \left(\frac{n^2}{r^2} - \beta^2\right)W_{n2} = 0 \tag{2.84}$$

and two identical equations for $W_n^*$ ($W_{n2}^*$ and $W_{n1}^*$). Equations (2.83) and (2.84) are at the form of Bessel's equations, which have the solutions

$$W_{n1} = A_n J_n(\beta r) + B_n Y_n(\beta r), \qquad W_{n2} = C_n I_n(\beta r) + D_n K_n(\beta r) \tag{2.85}$$

respectively. Here $J_n$ and $Y_n$ are the Bessel functions of first and second kind, respectively, and $I_n$ and $K_n$ are the modified Bessel functions of the first and second kind, respectively [37]. The mode shapes are determined by the coefficients $A_n$, $B_n$, $C_n$ and $D_n$ and they are solved using the boundary conditions. Thus the general solution of Equation (2.78) is

$$W(r, \theta) = \sum_{n=0}^{\infty} [\, A_n J_n(\beta r) + B_n Y_n(\beta r) + C_n I_n(\beta r) + D_n K_n(\beta r)]\, \cos\, n\theta$$

$$+ \sum_{n=0}^{\infty} [\, A_n^* J_n(\beta r) + B_n^* Y_n(\beta r) + C_n^* I_n(\beta r)$$

$$+ D_n^* K_n(\beta r)]\, \sin\, n\theta \qquad\qquad (2.86)$$

For solid circular plates, in order to avoid singularity of deflections and stresses at the origin (r=0), the terms, that are involving $Y_n$ and $K_n$ in the solution, must be discarded. In addition, if the boundary conditions are symmetrically applied about a diameter of the plate, then the second expression containing *sin $n\theta$* is not needed to represent the solution. Then, the n-th term of Equation (2.86) becomes

$$W_n(r, \theta) = [A_n J_n(\beta r) + C_n I_n(\beta r)]\, \cos\, n\theta \qquad\qquad (2.87)$$

for n = 0,1,....., $\infty$. A nodal line is the one which has zero deflection (i.e. $W_n = 0$), and represents the points or areas which remain in equilibrium position during any vibration [38]. For circular plates nodal lines are represented as either concentric circles or diameters. In addition to that, the nodal diameters are determined by $n\theta = \pi/2, 3\pi/2,....$

Depending on the frequency, main section of the wood, and wood species, the sand on the plate can be group in nodal lines. These nodal lines can be represented with some experimental efford, and the powder or the sand creates some patterns called Chladni patterns. The nodal lines create modal forms on the plates, and the modal shapes become more and more complex and tend to be similar regardless of species. Chladni patterns can be used to trace the evaluation of the mode shape through a number of geometric changes. There are some example Chladni patterns in Figure 2.7 below. As it can be seen on the figure that there are some symmetrical behaviors on the plates, this symmetry of modal shapes depends on the symmetry of the wood microstructure.
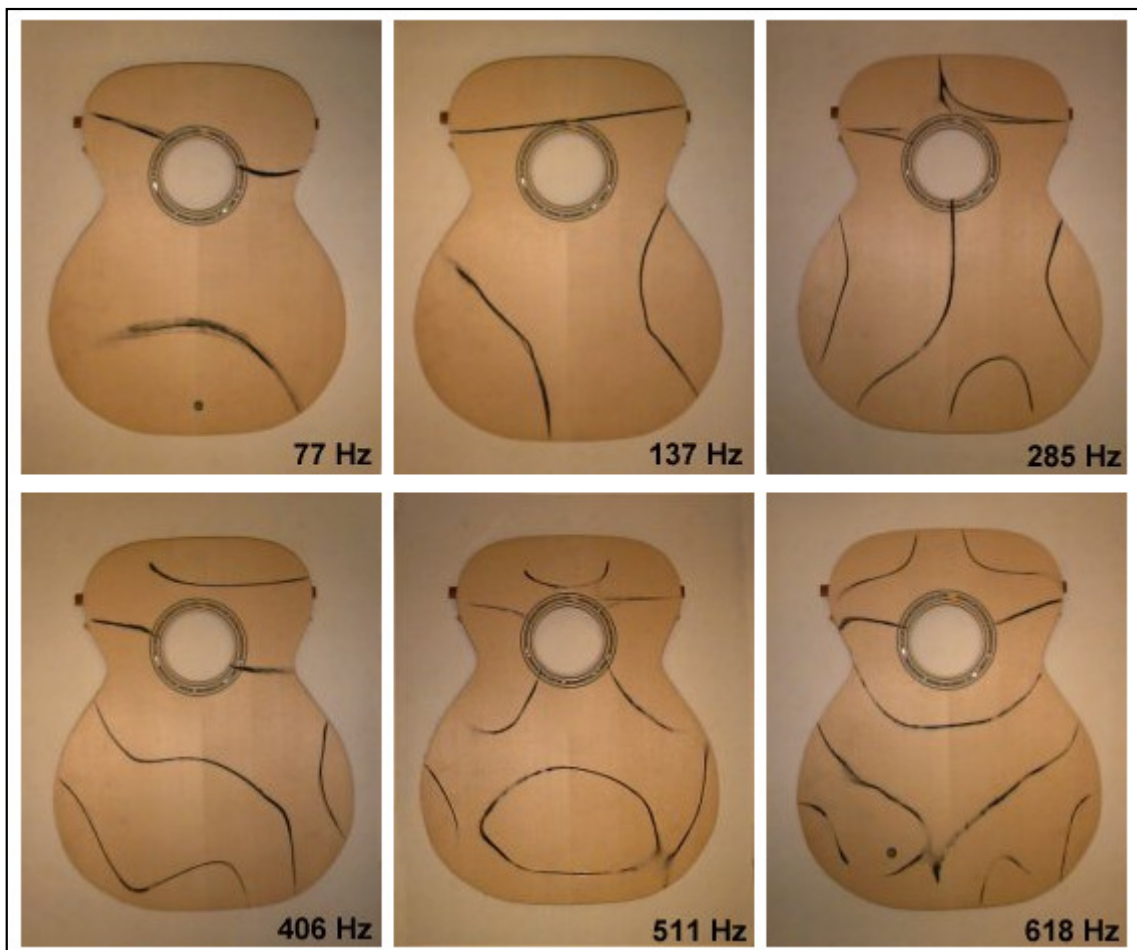
Figure 2.7. Some example Chladni patterns with different frequency values (Illustrations are taken from [39])

As the next step, the analytical solutions of a circular plate are obtained for two differents boundary conditions.

The clamped circular plate problem that is shown in Figure 2.4 is examined. For this case the boundary conditions are given as

$$W_n = 0 \quad , \quad \frac{\partial^2 W_n}{\partial r} = 0 \quad \text{at r} = \text{a for any } \theta \tag{2.88}$$

Using the equation (2.87) and (2.88), it is obtained that

$$\begin{bmatrix} J_n(\lambda) & I_n(\lambda) \\ J_n'(\lambda) & I_n'(\lambda) \end{bmatrix} \begin{pmatrix} A_n \\ C_n \end{pmatrix} = \begin{pmatrix} 0 \\ 0 \end{pmatrix} \tag{2.89}$$

where $\lambda = \beta a$ and the prime denotes differentiation with respect to the $\beta r$ expression. The determinant of the coefficient matrix in Equation (2.89) is set to zero for nontrivial solution

$$\begin{vmatrix} J_n(\lambda) & I_n(\lambda) \\ J_n'(\lambda) & I_n'(\lambda) \end{vmatrix} = 0 \tag{2.90}$$

Then expanding the determinant and using the recursion relations we obtain

$$J_n(\lambda)I_{n+1}(\lambda) + I_n(\lambda)J_{n+1}(\lambda) = 0 \tag{2.91}$$

which is called the frequency equation. The roots $\lambda$ of Equation (2.91) are said to be the eigenvalues, and are used to determine the frequencies $\omega$ [see Equation(2.79)].

$$\omega^2 = \frac{F\beta^4 + k}{I_o} = \frac{F\lambda^4 + ka^4}{a^4 I_o} \tag{2.92}$$

When $k = 0$, the Equation (2.92) reduces to this form:

$$\omega^2 = \frac{F\lambda^4}{a^4 I_o} \qquad or \qquad \lambda^2 = \omega a^2 \sqrt{I_o/F} \tag{2.93}$$

There are an infinite number of roots $\lambda$ of Eqn. (2.91) for each value of $n$ number, which represents the number of nodal diameters. For example, the roots in order of magnitude correspond with 1,2,...,m nodal circles when n = 0 (i.e. when the only nodal diameter is the boundary circle). The mode shape associated with $\lambda$ is determined using Eqn. (2.90)

$$\frac{A_n}{C_n} = -\frac{I_n(\lambda)}{J_n(\lambda)} \tag{2.94}$$

where $\lambda$ is the solution (i.e. root) of Equation (2.91). The radii of nodal circles $\zeta = r / a$ are determined from Equations (2.94) and (2.87)

$$\frac{J_n(\lambda\zeta)}{J_n(\lambda)} = \frac{I_n(\lambda\zeta)}{I_n(\lambda)} \tag{2.95}$$

Now, the simply supported circular plate problem that is shown in Figure 2.5 is examined. The boundary conditions $W_n$ and the bending moment about the $r = a$ is zero for this case at any $\theta$. In addition, $\partial^2 w_0/\partial\theta^2 = 0$ on the boundary. Using the Equation (2.87) and Equation (2.95) results in the following equations:

$$A_n J_n(\lambda) + C_n(\lambda) I_n(\lambda) = 0 \tag{2.96}$$

$$A_n \left[ J_n''(\lambda) + \frac{\nu}{\lambda} J_n'(\lambda) \right] + C_n \left[ I_n''(\lambda) + \frac{\nu}{\lambda} I_n'(\lambda) \right] = 0 \tag{2.97}$$

These equations lead to the frequency equation

$$\frac{J_{n+1}(\lambda)}{J_n(\lambda)} + \frac{I_{n+1}(\lambda)}{I_n(\lambda)} = \frac{2\lambda}{1 - \nu} \tag{2.98}$$

The mode shape can be determined using Equation (2.96) and (2.97)

$$\frac{A_n}{C_n} = -\frac{I_n(\lambda)}{J_n(\lambda)} \tag{2.99}$$

where $\lambda$ is a solution of Equation (2.98). So, the Equation (2.93) is also valid for the simply supported case but the values of $\lambda$ are different from the clamped case solution as it should be.

## 2.3. NUMERICAL IMPLEMENTATION OF THE THICK PLATE THEORY

The thin plate theory was first formulized by Kirchhoff in 1850's and his name is accociated with his name with this theory. Then Reissner [40] and Mindlin [41] made some relaxation of assumptions, and these modified theories extend the field of application of the thick plate theory. Then, this theory is accociated with the name of Reissner-Mindlin plate theory.

Two general assumptions are made for the thick plate theory. First and the most important assumption is that the sections normal to the middle plane remain plane during the deformation. Secondly, the direct stresses in the normal direction are small, i.e., of the order of applied lateral load intensities and the direct strains in that direction are negligable. It seems to have an inconsistancy case here; however, this is compansated by assuming a plane stress condition in each lamina. To explain the thick plate theory and its representation for finite element formulation, the study of Zienkiewizcz [42] is generally used. The general force resultants and the displacements for bending of a plate are given in Figure 2.8.
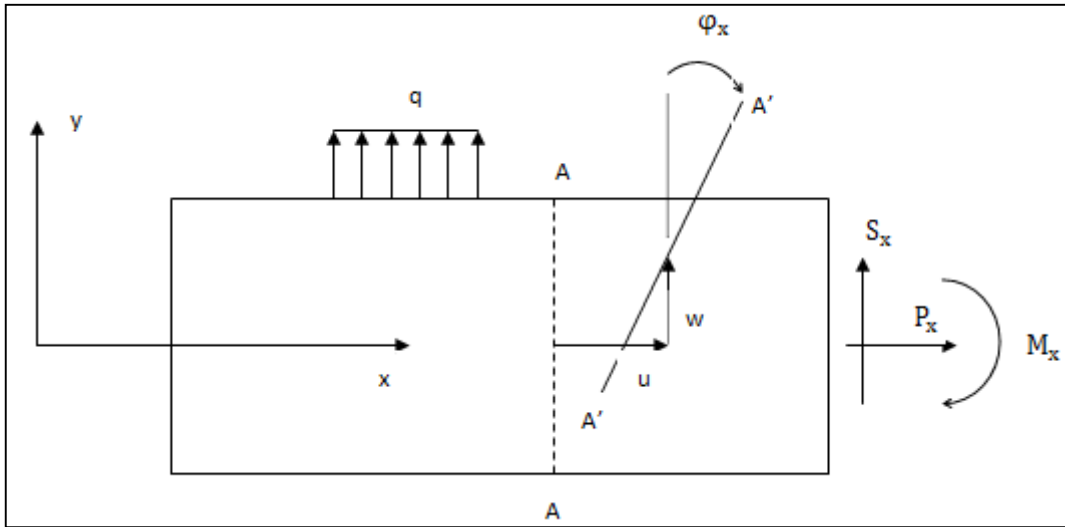
Figure 2.8. Force resultants and displacements for bending of a plate (Illustration is inspired from [42])

The stress resultants are obtained as

$$P_x = \int_{-t/2}^{t/2} \sigma_x \, dz = B \frac{\partial u}{\partial x} \tag{2.100}$$

$$S_x = \int_{-t/2}^{t/2} \tau_x \, dz = \kappa Gt \left( \frac{\partial w}{\partial x} + \varphi_x \right) \tag{2.101}$$

$$M_x = \int_{-t/2}^{t/2} \sigma_x \, z \, dz = F \frac{\partial \varphi_x}{\partial x} \tag{2.102}$$

where $P_x$ is the x-direction axial force, $S_x$ is the x-direction transverse shear force, $M_x$ is the x-direction bending moment, B is the in-plane plate stiffness, h is the thickness of the plate, $\kappa$ is the shear factor, and F is the bending stiffness and its representations are given below for rectangular plate as

$$F_1 = \frac{E_1 h^3}{12(1 - \nu_{12}\nu_{21})} \qquad (2.103)$$

$$F_2 = \frac{E_2 h^3}{12(1 - \nu_{12}\nu_{21})} \qquad (2.104)$$

$$F_{66} = \frac{G_{12} h^3}{12} \qquad (2.105)$$

for orthotropic elastic materials. Here, $\nu$ terms are the Poisson's ratios, E and G are the direct and the shear elastic modulus, respectively.

The basic difference between the thin and thick plate formulation is the presence of the shear term. In thin plate theory, the shear deformation is neglected and $G = \infty$ (or $\gamma_{xy}=0$) is put on the in Eqn (2.101). So the right-hand side of the equation becomes

$$\frac{\partial w}{\partial x} + \varphi_x = 0 \qquad (2.106)$$

Thus, in thin plate assumption the shear term becomes immaterial, and it is equivalent to say that the normals to the middle plane remain normal to it during deformation and is the same as the Bernoulli-Euler assumption for thin plates.

In general, the strains can be seperated into in-plane, i.e., bending components and transverse shear groups as given below:

$$\varepsilon = \begin{pmatrix} \varepsilon_x \\ \varepsilon_y \\ \gamma_{xy} \end{pmatrix} = z \begin{bmatrix} \partial/\partial x & 0 \\ 0 & \partial/\partial y \\ \partial/\partial y & \partial/\partial x \end{bmatrix} \begin{pmatrix} \phi_x \\ \phi_y \end{pmatrix} \equiv z\mathcal{L}\phi \qquad (2.107)$$

$$\gamma = \begin{pmatrix} \gamma_{xy} \\ \gamma_{yz} \end{pmatrix} = \begin{pmatrix} \partial w/\partial x \\ \partial w/\partial y \end{pmatrix} + \begin{pmatrix} \phi_x \\ \phi_y \end{pmatrix} = \nabla w + \phi \tag{2.108}$$

where $z$ is the normal direction that the transverse loading, q, is applied to. In addition to normal bending moments, a twisting moment is also defined by

$$M_{xy} = \int_{-t/2}^{t/2} z\,\tau_{xy}\mathrm{d}z \tag{2.109}$$

Introducing appropriate constitutive relations, all moment components can be related to displacement derivatives. For orthotropic elasticity the below equation can be written

$$\mathbf{M} = \begin{pmatrix} M_x \\ M_y \\ M_{xy} \end{pmatrix} = \mathbf{D}\mathcal{L}\phi \tag{2.110}$$

where $D$ matrix was represented before in Eqn (2.46).

Further, the shear force resultants are

$$\mathbf{S} = \begin{pmatrix} S_x \\ S_y \end{pmatrix} = \alpha(\nabla w + \phi) \tag{2.111}$$

Here the 2 by 2 matrix, $\alpha$, martix that includes the shear terms was defined before in Eqn (2.52) for orthotropic elasticity.

The governing equations of thick plate behaviour are completed by expressing the equilibrium relations with omitting the in-plane behaviour, and these are given at below:

$$\left[\frac{\partial}{\partial x}, \frac{\partial}{\partial y}\right] \begin{pmatrix} S_x \\ S_y \end{pmatrix} + q \equiv \nabla^T \mathbf{S} + q = 0 \tag{2.112}$$

$$\begin{bmatrix} \partial/\partial x & 0 & \partial/\partial y \\ 0 & \partial/\partial y & \partial/\partial x \end{bmatrix} \begin{pmatrix} M_x \\ M_y \\ M_{xy} \end{pmatrix} + \begin{pmatrix} S_x \\ S_y \end{pmatrix} \equiv \mathcal{L}^T \mathbf{M} + \mathbf{S} = \mathbf{0} \qquad (2.113)$$

The equations (2.110), (2.111), (2.112), and (2.113) are the basis from which the thick plate solution can start. To sum up, Eqn (2.110) is the moment constitutive equation in the form of $\mathbf{M}$ - $\mathbf{D}\mathcal{L}\,\phi = \mathbf{0}$ , Eqn (2.111) is the shear constitutive equation in the form of $\frac{1}{\alpha}\,\mathbf{S} - \phi - \nabla w = \mathbf{0}$, Eqn (2.112) is the shear equilibrium equation, and Eqn (2.113) is the moment equilibrium equation.

It is convenient to eliminate M from the equation set and write the system as three equations:

$$\mathcal{L}^T \mathbf{D}\mathcal{L}\phi + \mathbf{S} = \mathbf{0} \qquad (2.114)$$

$$\nabla^T \mathbf{S} + q = \mathbf{0} \qquad (2.115)$$

$$\frac{1}{\alpha}\mathbf{S} - \phi - \nabla w = \mathbf{0} \qquad (2.116)$$

This equation system can be reduced to an irreducible form and can serve as the basis on which a mixed discretization is built. As stated before, the problem becomes thin-plate problem when $\alpha$ is equal to infinity. On the other hand, if $\alpha$ is not equal to infinity as it in the thick plate assumption, it is easy to derive an alternative irreducible form. The shear forces can be eliminated from the above equations (2.114), (2.115), and (2.116) and this can be represented as set of two equaitons as given below:

$$\mathcal{L}^T \mathbf{D}\mathcal{L}\phi + \alpha(\nabla w + \phi) = \mathbf{0} \qquad (2.117)$$

$$\nabla^T [\alpha\,(\nabla w + \phi)] + q = 0 \qquad (2.118)$$

Thus an irreducible system corresponding to minimization of the total potential energy can be written as below by using the above equations (2.117) and (2.118):

$$\Pi = \frac{1}{2}\int_{\Omega}(\mathcal{L}\phi)^{\mathsf{T}}\mathbf{D}\mathcal{L}\,\phi\;d\Omega + \frac{1}{2}\int_{\Omega}(\nabla w + \;\phi)^{T}\,\alpha\,(\nabla w + \phi)d\Omega - \int_{\Omega}wq\;d\Omega$$
$$+ \Pi_{bt} = minimum$$

(2.119)

As it can easily be verified that the first term is simply the bending energy and the second the shear distorsion energy in the above term. This is clearly be seen that this irreducible equation is valid only for $\alpha$ in not equal to infinity case. Now, using the equations (2.117) and (2.118) the discretization of the terms included at the equations can be made clearly, and these procedures are shown at the next part of the study.

### 2.3.1. The Irreducible Formulation (Reduced Integration)

We first consider that standart isoparametric interpolation in which shape functions are used to interplolate both the element geometry and displacement field (or some other field variable). For this purpose, two displacement variables are approximated by shape functions and parameters, and these are given below:

$$\phi = N_{\phi}\acute{\phi} + N_{b}\Delta\acute{\phi}_{b}$$

(2.120)

$$w = N_{w}\hat{w} + N_{w\phi}\acute{\phi}$$

(2.121)

$$S = N_{s}\tilde{S}$$

(2.122)

Here, $\phi$ and $w$ are the approximation of $\theta$ and $w$ by independent interpolations of $C_0$ continuity. The notation abbreviated as $b$ is used for modes named bubble. The

approximation equations can be obtained directly by the use of the energy equation as given below:

$$\Pi = \frac{1}{2}\int_{\Omega}(L\phi)^{\mathrm{T}}DL\,\phi\;d\Omega - \frac{1}{2}\int_{\Omega}S^{\mathrm{T}}\,\alpha^{-1}Sd\Omega + \int_{\Omega}S^{\mathrm{T}}\,(\nabla w +\ \phi)d\Omega$$

$$- \int_{\Omega}\mathrm{wq}\;d\Omega + \Pi_{bt} = stationary \tag{2.123}$$

Then using the equations (2.120), (2.121), (2.122), and (2.123) the below formulation is written:

$$\partial\Pi = \int_{\Omega}\partial\,\phi^{\mathrm{T}}L^{\mathrm{T}}DL\phi\;d\Omega - \int_{\Omega}\partial S^{\mathrm{T}}\,\alpha^{-1}Sd\Omega + \int_{\Omega}\partial S^{\mathrm{T}}\,(\nabla w +\ \phi)d\Omega$$

$$-\int_{\Omega}\partial\mathrm{wq}\;d\Omega + \Pi_{bt}$$

$$= \int_{\Omega}\partial\,[(N_{\phi}\,\tilde{\phi})^{\mathrm{T}} +\ (N_{b}\,\Delta\tilde{\phi}_{\mathrm{b}})^{\mathrm{T}}]\,L^{\mathrm{T}}DL\,(N_{\phi}\,\tilde{\phi} + N_{b}\,\Delta\tilde{\phi}_{\mathrm{b}})\;d\Omega$$

$$- \int_{\Omega}\partial S^{\mathrm{T}}N_{s}^{T}\,\alpha^{-1}N_{\mathrm{s}}Sd\Omega + \int_{\Omega}\partial S^{\mathrm{T}}N_{s}^{T}\,(\nabla(N_{\mathrm{w}}\hat{w} + N_{\mathrm{w}\phi}\tilde{\phi}) + N_{\phi}\tilde{\phi} + N_{b}\Delta\tilde{\phi}_{\mathrm{b}})\;d\Omega$$

$$- \int_{\Omega}\partial\,(N_{\mathrm{w}}\hat{w} + N_{\mathrm{w}\phi}\tilde{\phi})\,\mathrm{q}\;d\Omega + \Pi_{bt} \tag{2.124}$$

$$= \partial\,\phi\left[\int_{\Omega}N_{\phi}{}^{\mathrm{T}}\,L^{\mathrm{T}}DL\,N_{\phi}\;d\Omega\ +\int_{\Omega}\Delta\tilde{\phi}_{\mathrm{b}}\,(N_{b}{}^{\mathrm{T}}\,L^{\mathrm{T}}DL\,N_{\phi})\;d\Omega\right]$$

$$+ \partial S[\int_{\Omega}N_{s}^{T}\alpha^{-1}\,N_{\mathrm{s}}\,d\Omega] + \int_{\Omega}N_{s}^{T}\,(\nabla N_{\mathrm{w}\phi} - N_{\phi})\,\phi\;d\Omega + \int_{\Omega}N_{s}^{T}\,\nabla N_{\mathrm{w}}\;\hat{w}\;d\Omega]$$

$$+ \partial\,\Delta\tilde{\phi}_{\mathrm{b}}\left[\int_{\Omega}N_{b}{}^{\mathrm{T}}\,L^{\mathrm{T}}DL\,N_{b}\;d\Omega\right] - \int_{\Omega}(N_{s}^{T}N_{b})\,S^{\mathrm{T}}\,d\Omega]$$

$$=\ K_{\phi\phi} + K_{b\phi} + K_{ss} + K_{s\phi} + K_{sw} + K_{bb} + K_{sb}$$

where

$$K_{\phi\phi} = \int_{\Omega}(LN_{\phi})^{T}D(LN_{\phi})d\Omega \tag{2.125}$$

$$K_{b\phi} = \int_{\Omega} (\mathrm{L}N_b)^T \mathrm{D}(\mathrm{L}N_b) \mathrm{d}\Omega \tag{2.126}$$

$$K_{bb} = \int_{\Omega} (\mathrm{L}N_b)^T \mathrm{D}(\mathrm{L}N_b) \mathrm{d}\Omega \tag{2.127}$$

$$K_{sw} = \int_{\Omega} N_s^T \nabla N_{w\phi} \mathrm{d}\Omega \tag{2.128}$$

$$K_{ss} = -\int_{\Omega} N_s \nabla \alpha^{-1} N_s \mathrm{d}\Omega \tag{2.129}$$

$$K_{s\phi} = \int_{\Omega} N_s^T [\nabla N_{w\phi} - N_\phi] \mathrm{d}\Omega \tag{2.130}$$

$$K_{sb} = -\int_{\Omega} N_s^T N_b \, \mathrm{d}\Omega \tag{2.131}$$

Therefore, the discretized problem is obtained.

To complete the formulization, these should be written in a standard finite element representation (i.e. $kd = f$ where $k$ is the stiffness matrix, $d$ is the displacement vector, and $f$ is the force vector.). Therefore, the final form of the equation is given below:

$$\begin{bmatrix} 0 & 0 & 0 & K_{sw}^T \\ 0 & K_{\phi\phi} & K_{b\phi}^T & K_{s\phi}^T \\ 0 & K_{b\phi} & K_{bb} & K_{sb}^T \\ K_{sw} & K_{s\phi} & K_{sb} & K_{ss} \end{bmatrix} \begin{pmatrix} \widetilde{w} \\ \widetilde{\phi} \\ \Delta\widetilde{\phi}_b \\ \widetilde{S} \end{pmatrix} = \begin{pmatrix} f_w \\ f_\phi \\ 0 \\ 0 \end{pmatrix} \tag{2.132}$$

As this can be noted here that only the forces ($f_w$ and $f_\phi$) due to transverse load $q$ adn boundary conditions are shown for simplicity.

# 3. VERIFICATION AND VALIDATION

Before starting the analysis using actual instrument geometry, it is first necessary to make some analysis using the finite element solver named as `FEAP` and compare the results with analytical ones. This process will also serve to ensure that the relevant problem description is entered correctly to corresponding input file and that finite element solver is utilized properly.

On the other hand, benchmarking studies are done for deformation, and vibration analyses using a circular geometry. The diagram depicting the organization of the benchmark studies is given in Figure 3.1.
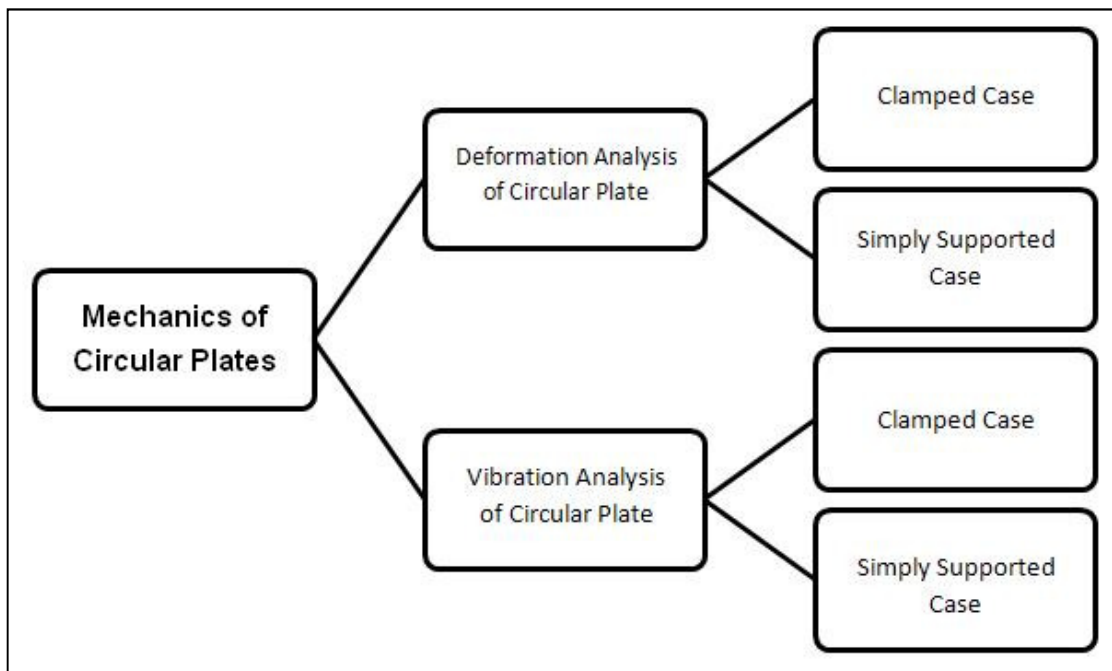


Figure 3.1. Schematic diagram of the benchmarking studies

The circular geometry is meshed using the a quarter circle for the deformation and a full circle for the vibrations analyses. This is due to the fact that some modes can dissapear if quarter circle geometry is used instead of a full circle.

Next, the procedure of solving problem using FEAP is briefly described, which is followed by the deformation results in Section 3.2 and the vibration results in Section 3.3.

## 3.1. STRUCTURE OF PROBLEM SOLVING USING FEAP

The general form of an input file is given as [43]:

```
FEAP * * Start record and title
    ....
Control and mesh description data
    ....
END
    ....
Solution and graphics commands
    ....
STOP
```

Initially, the input file starts with definitions of the general problem parameters as

```
FEAP
a1,a2,a3,a4,a5,a6
```

where $a1$ is the number of nodes, $a2$ is the number of elements, $a3$ is the number of material set, $a4$ is the spatial dimension of mesh, $a5$ is the number of degrees of freedom for each node, and $a6$ is the maximum number of nodes on any elements.

For the numerical part of the solution, the basic mesh form of the circular plate which consists of nodes and elements are generated. For the general finite elements included with the program, the mesh is described relative to a global Cartesian coordinate frame.

### 3.1.1. Control and Mesh Description Data

In the control and mesh description block the material properties, element properties, mesh properties such as element connectivity and model coordinate lists, and boundary conditions are specified.

The material sets are defined using the

```
MATErial
```

command. The next records after `MATE` consist of commands which describe the type of the element and the material parameters associated with the set. This record may also contain a material set number if more than one material set is used in the analysis. In our case, the plate element is used to model the expected structural behavior using the

```
PLATe
```

command. These types of elements are used for the small deflection analyses only and include bending and transverse shearing deformations. The model is formulated in terms of the force resultants which are computed by integration of stress components over the thickness of the plate. Each element is a quadrilateral with 4-nodes. The degrees of freedom for this kind of an element at each node are: The transverse displacement, $w$, and the rotations $\theta_x$ and $\theta_y$ about the coordinate axes; and the order of these are $\{w, \theta_x, \theta_y\}$ as shown in Figure 3.2.
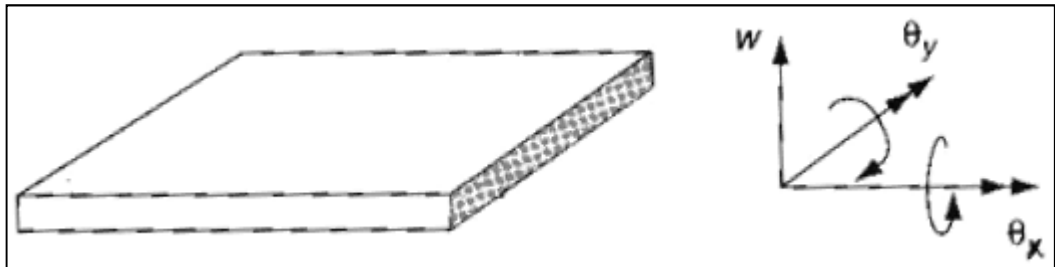


Figure 3.2. Representations of displacement, $w$ and rotations $\theta_x$, $\theta_y$ along a surface of a plate

In the benchmarking tests, the elastic isotropic material behavior is used. Finally the thickness of the plate, loading type, and the mass density values are inputted. The completed material set portion of the input file is written as

```
MATErial
 PLATE
 ELAStic isotropic e1 ν1 ! elastic modulus, Poisson's Ratio
 THICkness plate t1 ! plate thickness
 LOAD plate l1 ! uniform loading
 DENSity mass d1 ! mass density value
```

Note that however in the actual analyses results, the properties shown an orthotropic material are given as:

```
 ELAStic orthotropic e1 e2 e3 nu-12 nu-23 nu-31 g-12 g-23
 g-31
```

where the parameters represent the relevant coefficient of the stiffness.

Before meshing commands are executed, a set of parameters that are used in the further parts of the input file may be defined using the

```
 PARAmeter
```

command. This command also permits arithmetic calculations to be performed.

With respect to the problem geometry, the `COOR`, and `ELEM` commands are used to define the coordinates and the elements of the geometry, respectively. Some additional macros that also come with the `FEAP` provide extra functionality in building regular meshes. A block of nodes and elements is generated using the blending function approach for the circular geometry. In `FEAP`, the blending function meshes are created from a set of control points, which are said to be super-nodes; inputted using the `SNODe` command, edges inputted using the `SIDE` command and a description of the region using the `BLENd`

command. The coordinates for the super-nodes are given in Cartesian coordinate frame. The input file includes lines as:

```
SNODe
 N   X_N   Y_N   Z_N
  ....
```

where $N$ is the super-node number and is generated from 1 to the maximum number needed to describe all the blending functions. The super-nodes that are generated for the full circle geometry analyses are in shown in Figure 3.3.
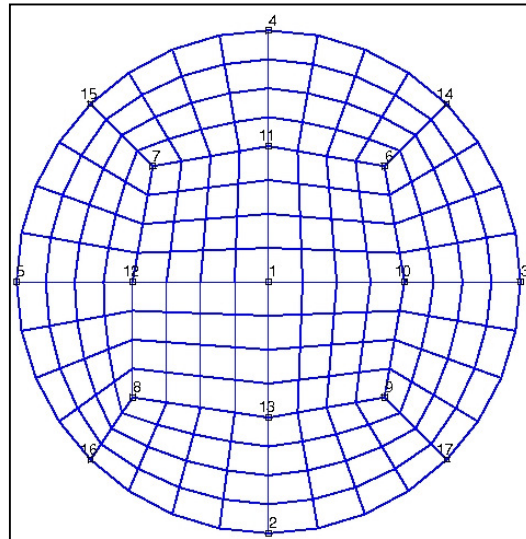


Figure 3.3. Super-nodes on the full circle geometry meshing

The sides of any surface and the edges of any solid to be generated by BLENd command should be prescribed. Only sides for non-straight or non-uniformly spaced increments such as a circular geometry need to be given. FEAP adds all straight uniformly spaced sides not given as input data automatically. The specification of sides using the SIDE command is given by the form:

```
SIDE
    Type   V1,V2,V3
```

where `Type` may either be specified on polar or Cartesian for the side, `V1` and `V2` are the super-node numbers for the ends (End 1 and End 2) of the sides, and `V3` is the intermediate node nearest End 1.

The blending function meshes are created from a set of control points (i.e. super-nodes), and 4-node quadrilateral elements are used for blending operation. The nodes and the quadrilateral elements defined by blending command is developed from a master element which is defined by an isoparametric mapping function in terms of the two natural coordinates. The first direction is defined along the direction of the first two super-nodes and the second direction along the direction of the first and fourth super-nodes.

`SURFace` option is used with the `BLENd` command and four vertex super-nodes specify the orientation of the region. The super-nodes should be given as an anti-clockwise sequence (right hand rule). The input is given as:

```
BLENd
SURFace inc-1 inc-2 Node1 Elem1 Mat1 Etype
     s1   s2   s3   s4
```

where `inc-1` is the number of nodal increments to be generated along 1-2 edge, `inc-2` is the number of nodal increments to be generated along 2-3 edge, `Node1` is the number to be assigned to first generated node in patch (first node is located at the same location as master node 1), `Elem1` is the number to be assigned to first element generated in patch, `Mat1` is the material identifier to be assigned to all generated elements in patch (default = 1), and *Etype* is the element type.

The value of a force or displacement is selected based on the boundary restraint code value active at the time of execution. Non-zero boundary restraint codes imply a specified displacement and zero implies a specific load. The boundary restraint codes are set using the

```
        BOUNdary codes
            N1    I1    R1    R2
```

command where `N1` is the node number restraint codes, `I1` is the increment of nodes for the next ones, `R1` and `R2` are the restrained codes for the boundaries.

For the boundary node of interest angle boundary conditions can be prescribed by specifying the angle in degrees. The data is written using the command

```
        ANGLe
            N1    I1    A1
```

where `N1` denotes the node number, `I1` is the increment for the next node, and `A1` is the value of the angle.

In relation with the boundary definitions, one should mention the `EBOUndary` command used to define the boundary conditions for modelling the lines of symmetry of the quarter circle geometry. The form of this command is

```
        EBOUndary
            N1    I1    B1    B2    B3
```

where `N1` is the number of nodes, `I1` is the increments in the node numbers, and `B1,B2,B3` are the boundary values (zero or non-zero) for the associated coordinates.

Finally, the `CANGle` command is used to enforce the change of coordinates for those nodes rotated by the `ANGLe` command.

## 3.1.2. Solution and Graphics Commands

`FEAP` performs solution steps based upon user specified comand language statements, and the program provides commands which can be used to solve problems

using standard algorithms. In order to enter the solution command language part of FEAP the user includes the BATCh command in the input file. The batch solution is terminated by the command END. Thus, the input file looks like:

```
BATCh
     LOOP
             .... ! Solution specification steps
     END
END
```

Next, some of the solution commands available in the program are described.

The solutions of problems by FEAP are obtained by computing residuals for the governing equations followed by a sequence of solution steps to reduce the size of the residual to a very small value. The residual for each step may be computed using the FORM command, which is placed on the top of the macros within a LOOP statement. When the value of residual completed in form falls below a threshold value defined as TOLErance the solution is thought to be converged and the program exists the loop. For structural problems like the one we are studying, the MASS command computes the inertia matrix. In order to form symmetric tangent arrays for use in an iterative solution, the command TANGent is used. This command computes the tangent stiffness matrix for the current solution. The general form of these commands is given below as:

```
LOOP
     FORM
     TANGent
     SOLVe
END
```

When the direct solution by a Gauss elimination algoraitm is used the tangent matrix is also factored into the form without pivoting as:

$$K_t = (UT)^t(DM)(UT) \qquad (3.1)$$

where $DM$ is a diagonal matrix, $UT$ is an upper triangular matrix, and $K_t$ is the tangent stiffness matrix.

The generalized linear eigenvalue problem can be stated as:

$$K_t\Phi = B\Phi\Lambda \qquad (3.2)$$

where $\Phi$ are the eigenvectors, $\Lambda$ is the eigenvalues. $\mathbf{B}$ has three options for the solution: $\mathbf{B} = \mathbf{M}$ the mass matrix, $\mathbf{B} = \mathbf{K_G}$ the geometric stiffness matrix, and $\mathbf{B} = \mathbf{I}$ an identity matrix. To solve this type of a problem the `SUBSpace PRINt n1 g1` command is used where the parameter `PRINt` results in an output of the subspace arrays, `n1` is the number of converged pairs requested and `g1` is the number of extra vectors to use for acceleration of the convergence.

The `SOLVe` command is used after the computation of the tangent matrix and a resudial in the solution of

$$K_t\Delta u = R(u) \qquad (3.3)$$

where u denotes the set of nodal displacements and Δu, the solution increment for the current step. Upon convergence the solution contains the generalized displacement at nodes. The numerical values for the nodal displacements at each node are calculated using the:

```
DISPlacement nodes n1 n2 inc
```

command where `n1` and `n2` define the fisrt and the last node to output and `inc` is the increment between node numbers.

The `STREss` command is used to list the stress results in elements `n1` to `n2` at increments of `n2`, and it is inputted as:

```
STRE,,n1,n2
```

The values at all points are reported with `STREss,ALL` command.

Finally, the issuing of the command `PLOT` from an interactive mode causes input to be requested for plot commands. In the `BATCh` mode, the specific command for plotting is given as:

```
PLOT type v1 v2 v3
```

where type defines the plot command and `v1`, `v2`, and `v3` are the parameters needed to perform te plot.

After preparing the general input file we are ready to begin the deformation and vibration analyses for various kinds of mesh profiles for a circular geometry.

## 3.2. DEFORMATION ANALYSES

### 3.2.1. Isotropic Case

For the deformation analysis of the circular geometry, the analytical solution of the problem given in the Section 2.2 is compared with the finite element results.

The problem is meshed using a quarter circular geometry having a radius of 2 mm. Plate element is selected as the element type. A uniformly distributed loading of 10 N/m$^2$ is applied in the vertical direction, and the material properties are defined as Elastic modulus = 210000 MPa and Poisson's ratio = 0.3 wheras its thickness / radius ratio is kept at 0.025.

Necessary boundary conditions are entered as input for both clamped and simply supported cases. Finally, the finite element program is run for these cases.

The numerical deformations at nodes are compared with analytical curves given in Eqn (2.65) and (2.66) for the clamped and the simply supported cases, respectively. As it can be seen easily from Figure 3.4 the analytical results match perfectly with the finite element calculations. The input macro files generation process, is thus verified for deformational type analyses.
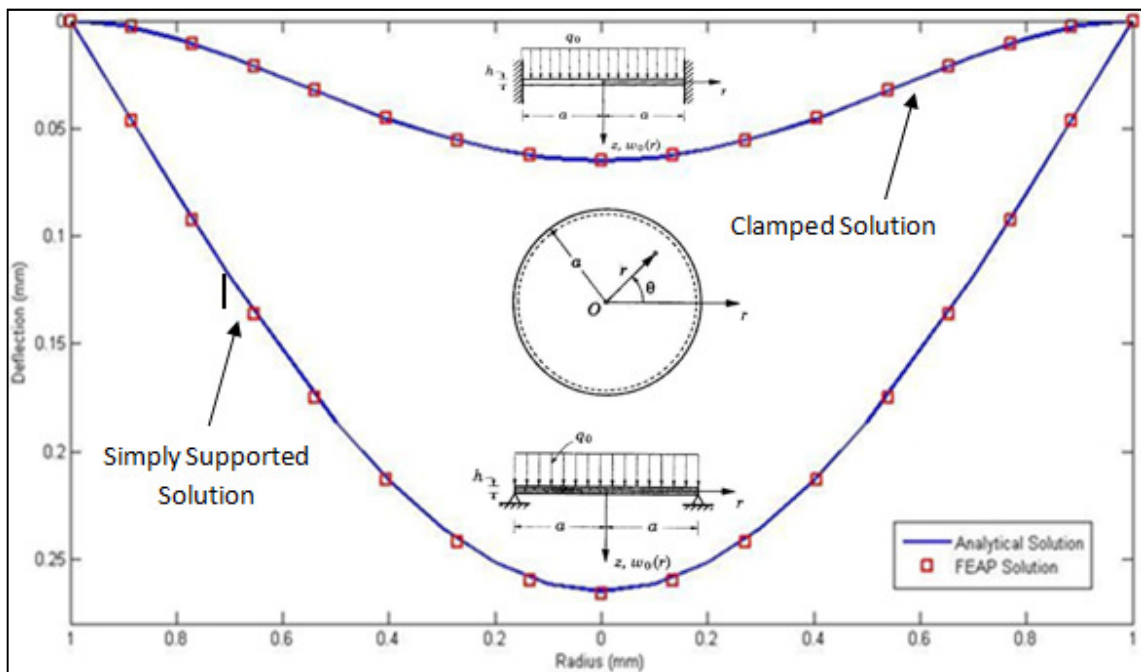


Figure 3.4. Validation of deformation obtained from the finite element model with the analytical result

At this point, a verification analysis is performed through a sensitivity study, to assess the accuracy of the numerical procedure. The deflection value of center of the circle from the analytical solution is compared to numerical solutions with four different mesh densities. A super-node, which can be seen in Figure 3.3 as the node number 6, is defined at the middle of the quarter circle for each of them. Then four different meshed geometries are classified by average element size numbers (n). For instance, the tetragonal shape can

be seen in yellow colors in Figure 3.5 for n = 2 (i.e. each side of the tetragonal shape, whose one corner is at the middle super-node, has two portions).
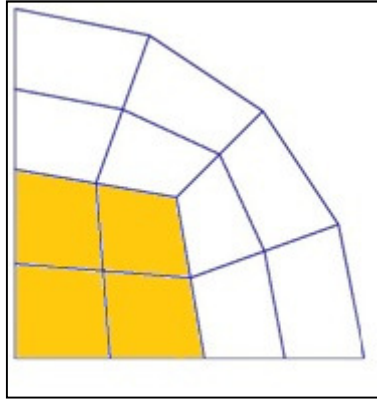


Figure 3.5. A sample mesh to show the average element size (n)

The geometries are meshed for n = 1, n = 2, n = 4, and n = 8 as shown in Figure 3.6. At each step, the mesh density value is doubled so that the order effect of mesh sizing on the error can be analysed in a systematic manner.
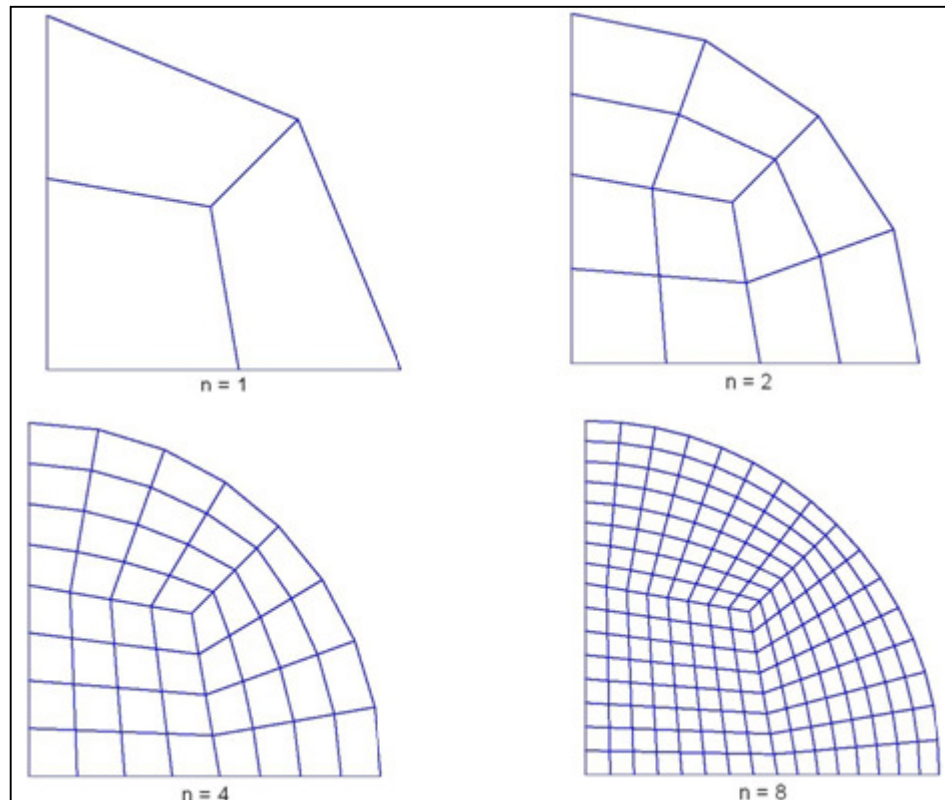
Figure 3.6. Four different mesh densities

The deflection values of the circle's center points are listed in the Table 3.1 and Table 3.2 for clamped and simply supported cases respectively. Accepting the analytical solution to be the true value, the errors are computed and listed in the below tables. Two types of error calculation is executed: true and approximate. The approximate error is calculated between meshes having two consecutive values of n while the true error is computed between the analytical value and the numerical value.

Table 3.1. Sensitivity Analysis for the Clamped Case

|  | Analytical | n = 1 | n = 2 | n = 4 | n = 8 |
|---|---|---|---|---|---|
| Deflection Value (mm) | 0.065000 | 0.050098 | 0.061878 | 0.064804 | 0.065530 |
| True Error (mm) | - | 0.014902 | 0.003122 | 0.000196 | - 0.000530 |
| Approximate Error (%) | - | 19.04 | 4.52 | 1.11 | - |
| Error Ratio | - | - | 4.21 | 4.07 | - |

Table 3.2. Sensitivity Analysis for the Simply Supported Case

|  | Analytical | n = 1 | n = 2 | n = 4 |
|---|---|---|---|---|
| Deflection Value (mm) | 0.26500 | 0.27042 | 0.26701 | 0.26609 |
| True Error (mm) | - | - 0.00542 | - 0.00201 | - 0.00109 |
| Approximate Error (%) | - | - 1.28 | - 0.35 | - |

Since the instrument that is being analysed has clamped boundary conditions, we did not only calculate the true and approximate errors but also checked the ratio between the two consecutive approximate errors (this ratio is given in the fourth row of the Table 3.1) for clamped case analyses. This error ratio values should be almost equal to each other for numerical reasons, and this sensitivity analyses show that we can handle the solution of any clamped conditioned problem using FEAP since the values (4.026, 4.030) are almost equal. Figure 3.7 shows the deflection values of the center point of the circle by the average element size numbers for clamped and simply supported cases using the logarithmic plot.
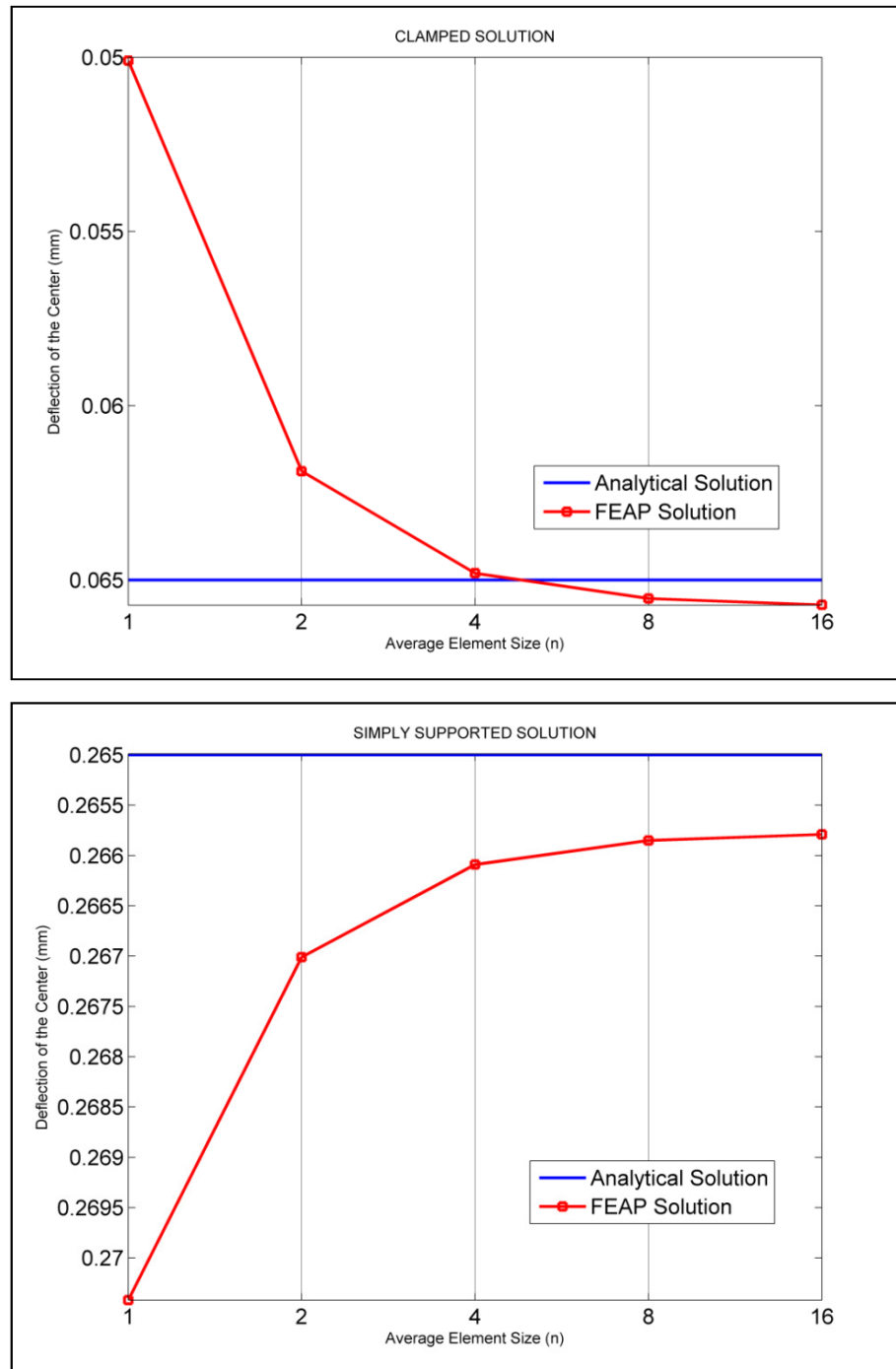
Figure 3.7. Deflection values of the center versus average element size number (n)

### 3.2.2. Orthotropic Case

For the deformation analysis of a material which has orthotropic behavior, a cantilever beam problem, whose analytical solution exists, is solved using two commercial finite element solvers: ANSYS and FEAP. The orthotropic material is chosen to be a wooden material, Spruce Sitka. The engineering parameters of the spruce sitka is given in Appendix B.

The geometry of the problem is given in Figure 3.8. As it can be seen on the figure that the problem is fixed supported (clamped) with the uniformly distributed load. The numerical values of the expressions at the geometry are selected as w = 10 N/m$^2$, L = 1.38 m, b = 0.32 m, h = 0.004 m for benchmarking analysis.
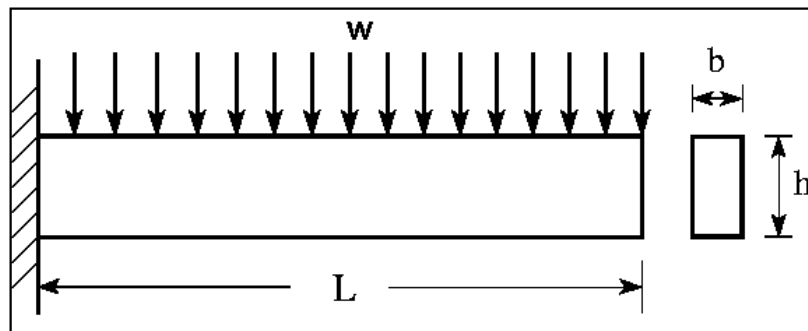


Figure 3.8. Cantilever beam geometry for the orthotropic case solution

As it is previously given at the theory part of the study, the analytical solution formula for the maximum deflection (i.e. deflection at the tip) is given below:

$$w_{max} = \frac{w * L^4}{8 * E_L * I} \tag{3.4}$$

where $I = (1/12)*b*h^3$.

Since two finite element solvers are used for the numerical solution of the problem, the number of elements should be equal for mesh models for an accurate comparison of the results. To do that, the average element size is selected as 0.01m for ANSYS solver. Thus the total number of elements is (1.38 / 0.01) * (0.32 / 0.01) = 4416. Similarly, the parameters (n1, and n2) in FEAP's input file are defined as 138, and 32 respectively so that the same number of elements value is obtained. The meshed view of the cantilever beam with 4416 elements is shown in Figure 3.9.
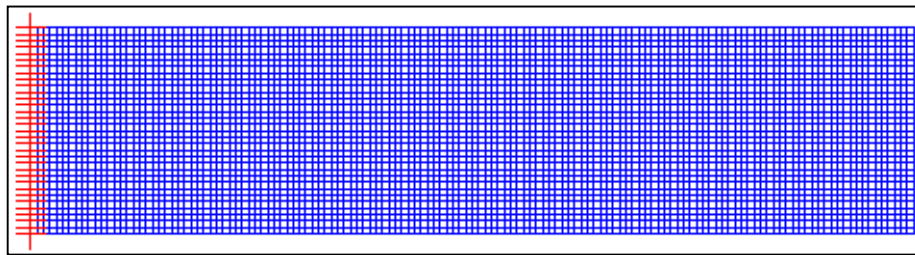


Figure 3.9. The meshed view of the cantilever beam

Plate element is selected as the element type for FEAP solver, and SHELL281 is selected for ANSYS program. The input sequence for the material properties parts is given below Table 3.3:

Table 3.3. Input file sequence of FEAP and ANSYS for orthotropic materials

|  | Input File Sequence for the Orthotropic Materials | | | | | | | | |
|---|---|---|---|---|---|---|---|---|---|
| FEAP | $E_L$ | $E_T$ | $E_R$ | $\nu_{LT}$ | $\nu_{TR}$ | $\nu_{RL}$ | $G_{LT}$ | $G_{TR}$ | $G_{RL}$ |
| ANSYS | $E_L$ | $E_T$ | $E_R$ | $\nu_{LT}$ | $\nu_{TR}$ | $\nu_{LR}$ | $G_{LT}$ | $G_{TR}$ | $G_{LR}$ |

The deflection results at the free end of the cantilever beam (the region where maximum deflection happens) is calculated for analytical solution with the formula given above, using FEAP, and using ANSYS. The result for the analytical solution is found as 73.27 mm. The numerical solutions are 72.58 mm (0.95 %), and 72.60 mm (0.46 %) for using FEAP, and ANSYS, respectively. The error values in percentage are given in the

paranthesis of each of the numerical solution. It is clearly being seemed that the numerical solutions for both finite element solvers are almost same with the analytical solution.

## 3.3. VIBRATION ANALYSES

### 3.3.1. Isotropic Case

#### 3.3.1.1. Clamped Boundary Condition

For the vibration analysis of the circle geometry for isotropic case, the analytical analyses of the problems given in the Section 2.2 are compared with the finite element results. The analyses of problem using FEAP are performed for the case whose average element size equals to eight.

For the finite element analysis, the material properties are defined as Elastic modulus = 210000 Pa and Poisson's ratio = 0.3. Its thickness value (h) is 0.05 mm, and its mass density ($\rho$) is 350 kg/m$^3$. The circle has the same radius value, 2 mm, as it is in the deformation analysis. The governing equations for the analytical solution process is given as follows (taken from the Eqn (2.93)):

$$\lambda^2 = \omega * a^2 * \sqrt{I/F} \qquad (3.5)$$

where $I = \rho*h$ is the principal inertia, and F is the bending stifness and its formula is

$$F = {E * h^3}/{12 * (1 - \nu)} \qquad (3.6)$$

For different values of m and n, there correspond a unique frequency $\omega_{mn}$ and the mode shape. The smallest value of $\omega_{mn}$ is said to be the fundamental frequency. It is not easy to find the lowest natural frequncy value when the rotatory inertia is not neglected.

For most plates (like the one we have) with thickness to side ratio value is under 0.1, the rotatory inertia can be neglected.

After entering the values to the above equation, we obtain:

$$\omega = 0.3706 * \lambda^2 \qquad (3.7)$$

To calculate $\lambda^2$ values, the square roots of eigenvalues (rad/t) are noted from the output file of the finite element solver for clamped case.

At Table 3.4, n denotes the number of nodal diameters and m is the number of nodal circles, not including the circle r = a. The $\lambda^2$ values are listed in Table 3.4 to make a comparison between the analytical and the numarical solutions.

Table 3.4. Comparison of $\lambda^2$ values with different combinations of nodal diameter (n), and nodal line for clamped boundary conditions

|  |  | m = 0 | m = 1 | m = 2 | m = 3 |
|---|---|---|---|---|---|
| n = 0 | Analytical Solution | 10.21 | 21.26 | 34.88 | 51.04 |
|  | Numerical Solution | 10.22 | - | 34.65 | 50.54 |
| n = 1 | Analytical Solution | 39.77 | 60.82 | 84.58 | 111.01 |
|  | Numerical Solution | 39.53 | 60.22 | - | - |

Here, it is seen that the calculated values of $\lambda^2$ matches well with the analytical results. So, every matching number shows us a different mode shape of this geometry. From using the output information of the finite element results, we are able to draw the mode shapes. Thus, we have opportunity to compare these with the mode shapes with the mode shape figures that are given in the referenced book. In Figure 3.10, the nodal diameters and the nodal circles can be seen for the several mode shapes. These mode shape figures are given below:
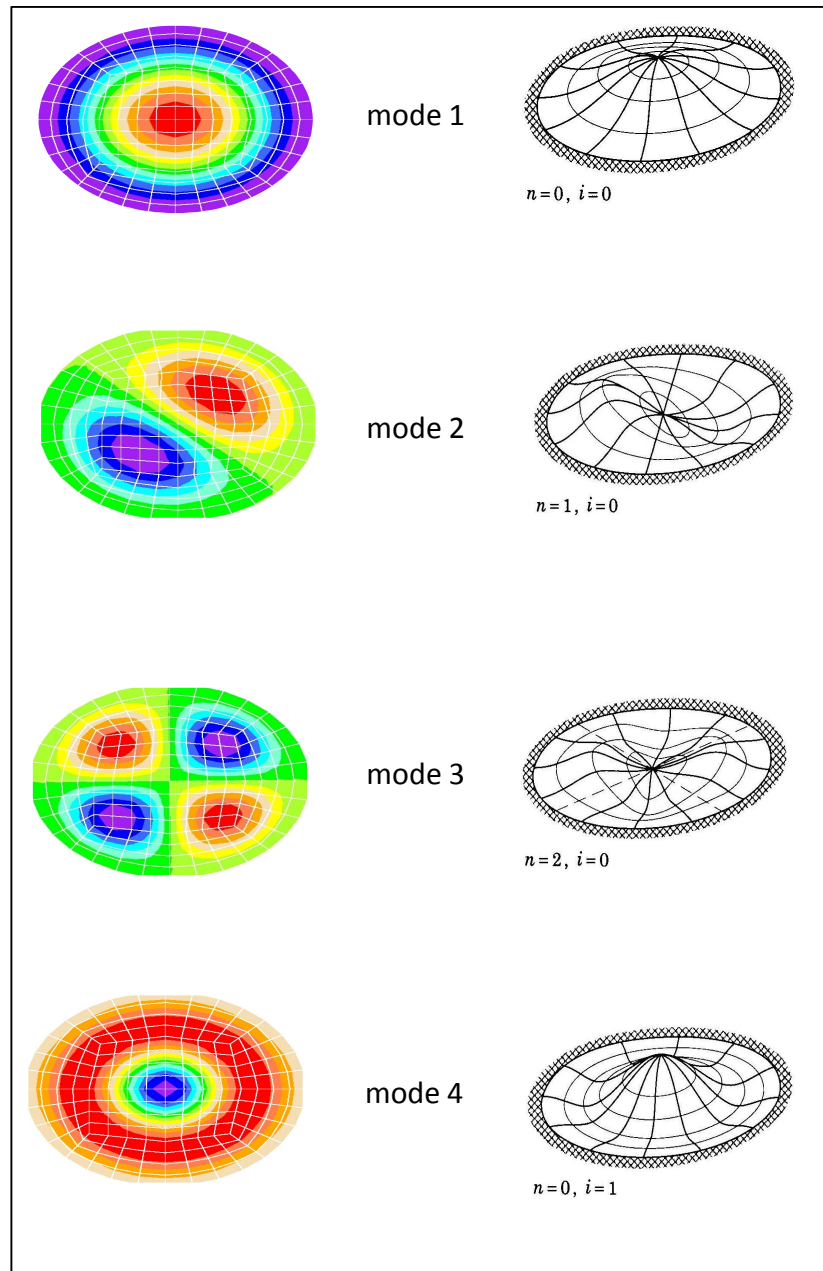
Figure 3.10. Mode shapes that are obtained from the analytical and finite element results

(Illustrations are taken from [36])

### 3.3.1.2. Simply Supported Boundary Condition

Same procedure of the clamped solution case is done for the simply supported solution too. The $\lambda^2$ values differ from the clamped case solution as it is expected.

$$\lambda^2 = \omega * a^2 * \sqrt{I/F} \tag{3.8}$$

After entering the values to the above equation, we obtain:

$$\omega = 0.3706 * \lambda^2 \tag{3.9}$$

To calculate $\lambda^2$ values the square root of eigenvalues (rad/t) values are noted from the output file of the finite element solver for simply supported case.

At Table 3.5, n denotes the number of nodal diameters and m is the number of nodal circles, not including the circle r = a. The $\lambda^2$ values are listed in the table to make a comparison between the analytical and the numarical solutions.

Table 3.5. Comparison of $\lambda^2$ values with different combinations of nodal diameter (n), and nodal line for simply supported boundary conditions

|  |  | m = 0 | m = 1 | m = 2 |
|---|---|---|---|---|
| n = 0 | Analytical Solution | 4.98 | 13.94 | 25.65 |
|  | Numerical Solution | 4.91 | 13.82 | 25.34 |
| n = 1 | Analytical Solution | 29.76 | 48.51 | 70.14 |
|  | Numerical Solution | 29.55 | 48.03 | - |

Here, it is seen that the calculated values of $\lambda^2$ matches well with the analytical results as it is in the clamped case.

## 3.2.2. Orthotropic Case

For an orthotropic case analysis, a rectangular clamped plate problem is selected from page 413 of reference [36]. The problem geometry is given Figure 3.11.
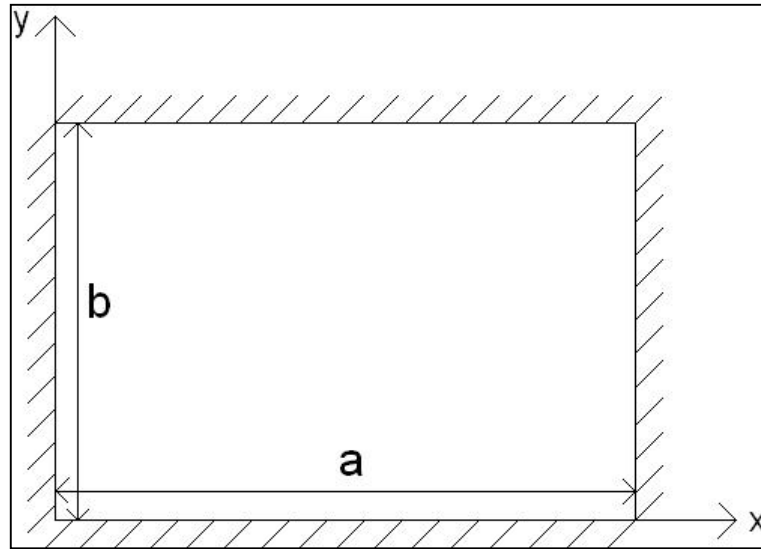
Figure 3.11. 4-sided rectangular clamped plate with dimensions a and b

These material properties are selected for analytical solution to determine the frequencies of this clamped plate for the orthotropic case: $E_1 = 10E_2$, $G_{12} = 0.5\ E_2$, $v = 0.25$. Although these indicate that the plate does not have a fully orthotropic behavior, the frequency solutions using these can give a general idea about the vibrational behavior of the plate.

Using the same equation for the isotropic case, the frequencies can be determined:

$$\lambda^2 = \omega_{mn} * a^2 * \sqrt{I/F} \tag{3.10}$$

where

$$F = \frac{E_2 * h^3}{12 * (1 - v_{12} * v_{21})} \tag{3.11}$$

Analytical solution is performed for two different plate aspect ratios ($\frac{a}{b} = \frac{0.6\ m}{0.4\ m} = 1.5$; $\frac{a}{b} = \frac{0.6\ m}{0.3\ m} = 2$) using the values of $E_1 = 108.2*10^8$ N/m$^2$, $E_2 = 4.7*10^8$ N/m$^2$, $\rho = 300$

kg/m$^3$, h = 0.005 m, $\nu$ = 0.25. The numerical solution is performed using only FEAP. Since input file of FEAP requires nine values for defining an orthotropic material, the values which are not defined by the analytical solution are assumed. The values of the orthotropic material are listed for the numarical solution: $E_L$ = 108.2*10$^8$ N/m$^2$, $E_T$ = 4.7*10$^8$ N/m$^2$, $E_R$ = 8.4*10$^8$ N/m$^2$, $\nu_{LT}$ = $\nu_{TR}$ = $\nu_{RL}$ = 0.25, $G_{LT}$ = $G_{TR}$ = $G_{RL}$ = 5.8*10$^8$ N/m$^2$. The analytical and the numerical solutions for two different aspect ratios are listed at the Table 3.6.

Table 3.6. Comparison of the first four natural frequencies of the clamped rectangular plate problem for the different aspect ratios

| $\omega_{mn}$ values for the first four natural frequencies (rad / s) | | | | | |
|---|---|---|---|---|---|
| | | a / b = 1.5 | | a / b = 2 | |
| m | n | Analytical | Numerical | Analytical | Numerical |
| 1 | 1 | 746.2 | 721.9 | 981.7 | 950.4 |
| | 2 | 1363.6 | 1306.3 | 1873.1 | 1784.4 |
| 2 | 1 | 1729.3 | 1640.8 | 2209.9 | 2109.3 |
| | 2 | 2161.8 | 2064.8 | 2846.7 | 2722.6 |

Since the analytical solution approach does not include all nine parameters of the orthotropic material, the results obtained from the numerical solution are slighly different from the analytical ones. The difference between the analytical and the numerical solutions is approximately 3-4 percent. This is an acceptable error and, thus, this indicates that the frequency solution of the general orthotropic modelling of any problem using FEAP ends up reliable results. In addition, the mode shape figures for the first four frequency that are obtained from numerical analyses are given in Figure 3.12.
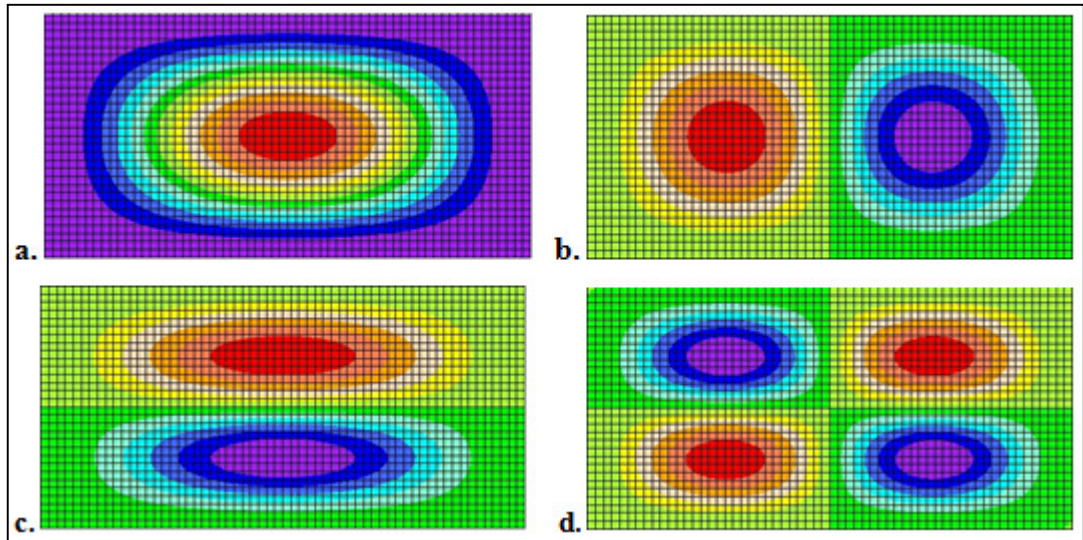
Figure 3.12. Mode shapes for the first four frequencies of the 4-sided clamped rectangular plate geometry for the orthotropic case using FEAP (for a / b =2)

# 4. RESULTS

In this chapter, the numerical experimental results are given for various types of cases. As given in Figure 2.3, the effects of variation of radial offset parameter to the results are the most important effort for our study. Besides the radial offset parameter, the tangential offset is other important value for the analyses. The representation of the radial offset and the tangential offset is given in Figure 4.1 as the top view and in Figure 4.2 as the isometric view.
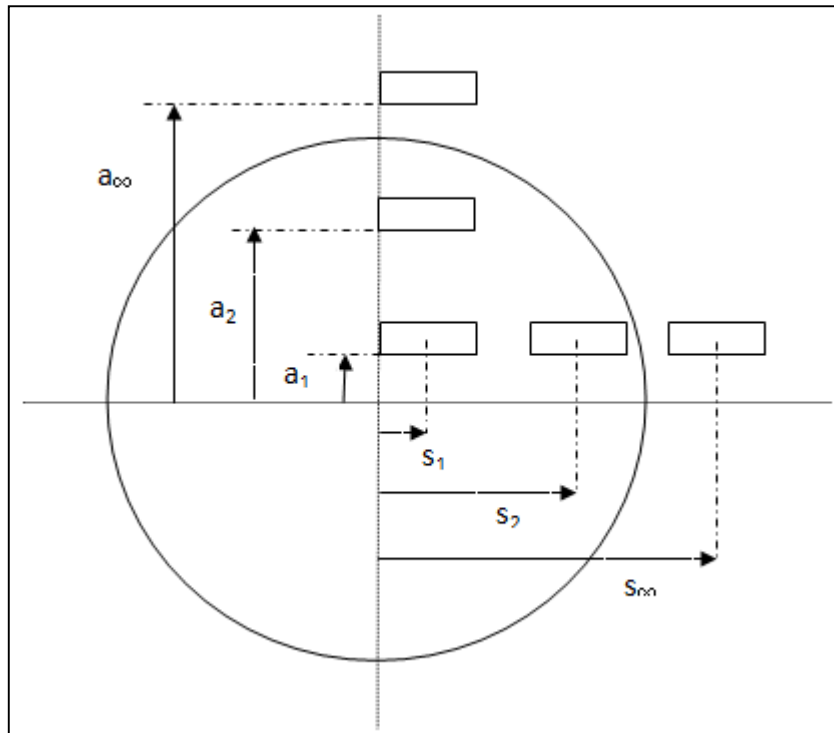


Figure 4.1. Radial offset distance, *a*, and tangential offset distance, *s*, from top view
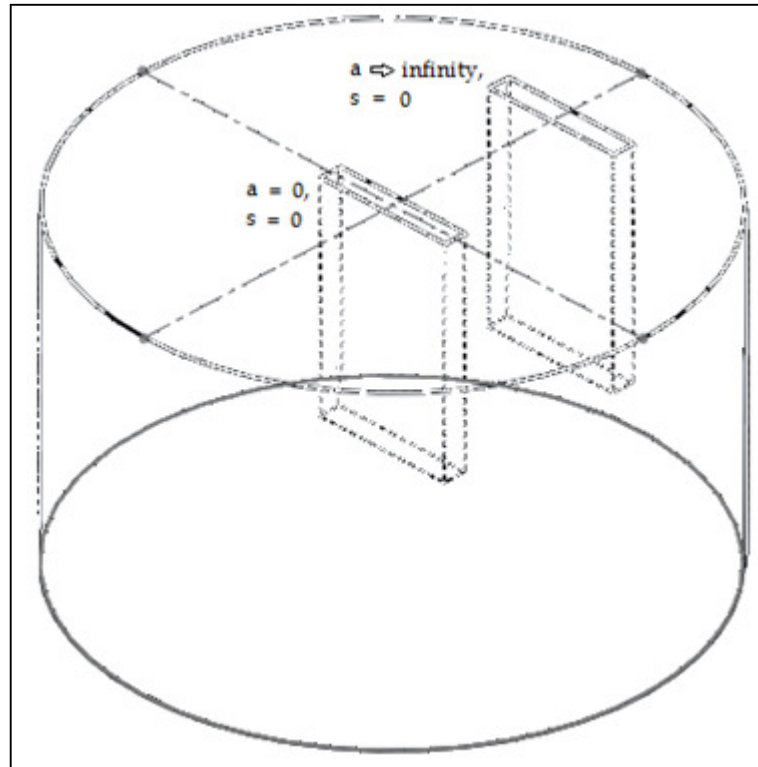
Figure 4.2. The cutting plane described as a function of radial offset, *a*, from the centroidal axis. Two different cases are examined and these are shown in isometric view

Figure 4.1 shows the radial offset distances, *a*, and the tangential offset distances, *s*, for a couple of configurations. Radial offset is the perpendicular distance between the plane of cut and the longitudinal axis, while the tangential offset is the distance measured in-plane between the centroids of the log and the plate. Figure 4.2 is given as to show the longitudinal cut plates in isometric view.

To summarize the analyse types, effect of the radial offset, effect of the tangential offset, effect of the geometry, and the effect of the wood type are shown to examine the variation of frequency response. The analyses are done using spruce sitka and clamped boundary condition. Now, each of these analyses is studied in sequence.

## 4.1. EFFECT OF RADIAL OFFSET

In Figure 4.4, we demonstrate the variation of frequency response with the radial offset of cutting plane for the longitudinal axis of the wood log. First five eigenvalues are plotted seperately. At this case, a square plate with side length 0.3545 m is cut from center of the wood (i.e. tangential offset distance = 0). All five eigenvalues show similar behavior. Mesh density is taken as 100 by 100 for this case. For the very small values of radial offset distance ($10^{-7}$ m, $10^{-5}$ m, $10^{-4}$ m), the frequency values are increasing up to a certain value, and for values around 0.001, 0.01 the frequency values decreases rapidly. Then, it behaves like a V-shaped curve for the values between 0.01 m and 1 m.

## 4.2. EFFECT OF TANGENTIAL OFFSET

In Figure 4.5, frequency behavior of a square plate with side length 0.3545 m and thickness 0.005 m is demonstrated as a function of tangential offset with varying radial offset distance. Two cases are examined for the analyses: first is $s = 0$ case and second is $s = 0.5 \times b$ case. Analyses are done for the first five eigenvalues and mesh density is taken as 100 by 100. For the ease of comparison, the radial offset distances of each case are taken as equal to each other. Similarly, V-shaped behavior exists at the definite interval of radial offset values (0.01 m to 1 m). As mentioned before that the most important behavior to be examined for us is the curve's V-shaped behavior so that we need to focus at this portion carefully. To do that, this portion is zoomed for all five cases of eigenvalues, and these plots are given in Figure 4.6.

## 4.3. EFFECT OF GEOMETRY

In Figure 4.7, the frequency values are compared with varying radial offset distance for two different geometries: one is a square plate with side length 0.3545 m, and the other one is a circle plate with radius 0.2 m. Their thickness values are both 0.005 m. Their volumes are selected to be equal to each other so that amount of material are equal for both cases and the comparison analyses would be rational to be performed. Mesh density is taken as 100 by 100 for square plate, while the number of total element of the circular mesh is taken as 10800. Mesh and boundary condition plot of clamped circular plate is given in Figure 4.3 below:
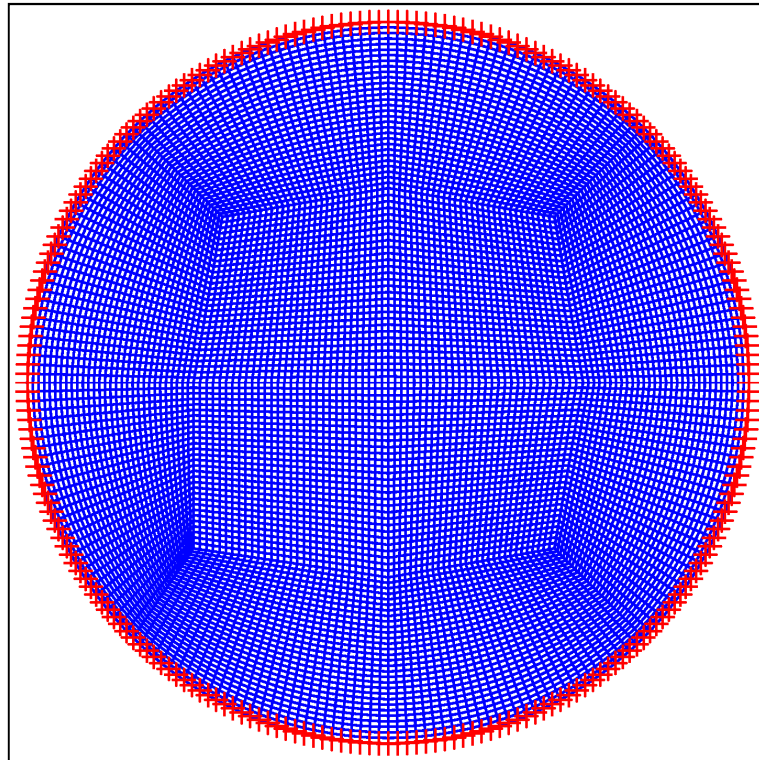
Figure 4.3. Circular mesh showing the boundary conditions in red colour. Total number of elements for this mesh is 10800

Like the previous cases, the plots are zoomed at the portion that the curve draws a V-shaped behavior. These plots are given in Figure 4.8a, Figure 4.8b, Figure 4.8c, Figure 4.8d, and Figure 4.8e.

## 4.4. EFFECT OF WOOD TYPE

In Figure 4.9, the frequency values of two different types of woods- balsa and spruce sitka- with varying radial offset distance value are compared. A square plate with side length 0.3545 m and thickness 0.005 m is used for the analyses. It is clearly be seen that the frequency values of spruce sitka analyses are higher than the values of balsa analyses for all five cases of interest. The first examined frequency value of spruce sitka case is nearly doubled the values of balsa values at each of the five cases. The zoomed plots are given in Figure 4.10a, Figure 4.10b, Figure 4.10c, Figure 4.10d, and Figure 4.10e.
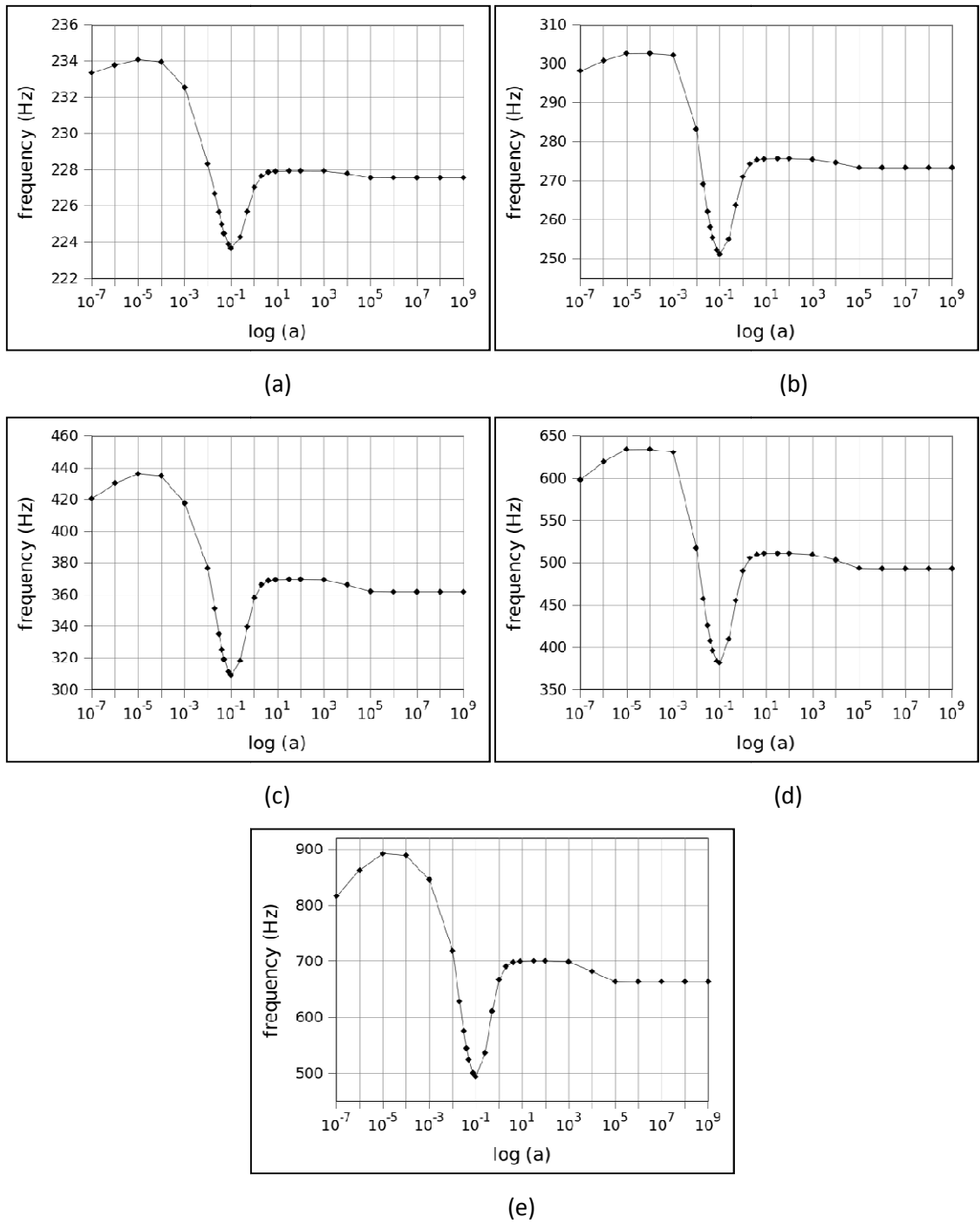
Figure 4.4. The frequency behavior of a square plate with side lenght 0.3545 m and thickness 0.005 m as a function of the radial offset. Figures (a), (b), (c), (d), (e) shows the first, second, third, fourth, and fifth eigenvalues, respectively

(a)

(b)

(c)

(d)

(e)

Figure 4.5. The frequency behavior of square plate with side lenght 0.3545 m and thickness 0.005 m as a function of tangential offset. Figures (a), (b), (c), (d), (e) shows the first, second, third, fourth, and fifth eigenvalues, respectively

(a)

(b)

(b)

(d)

(e)
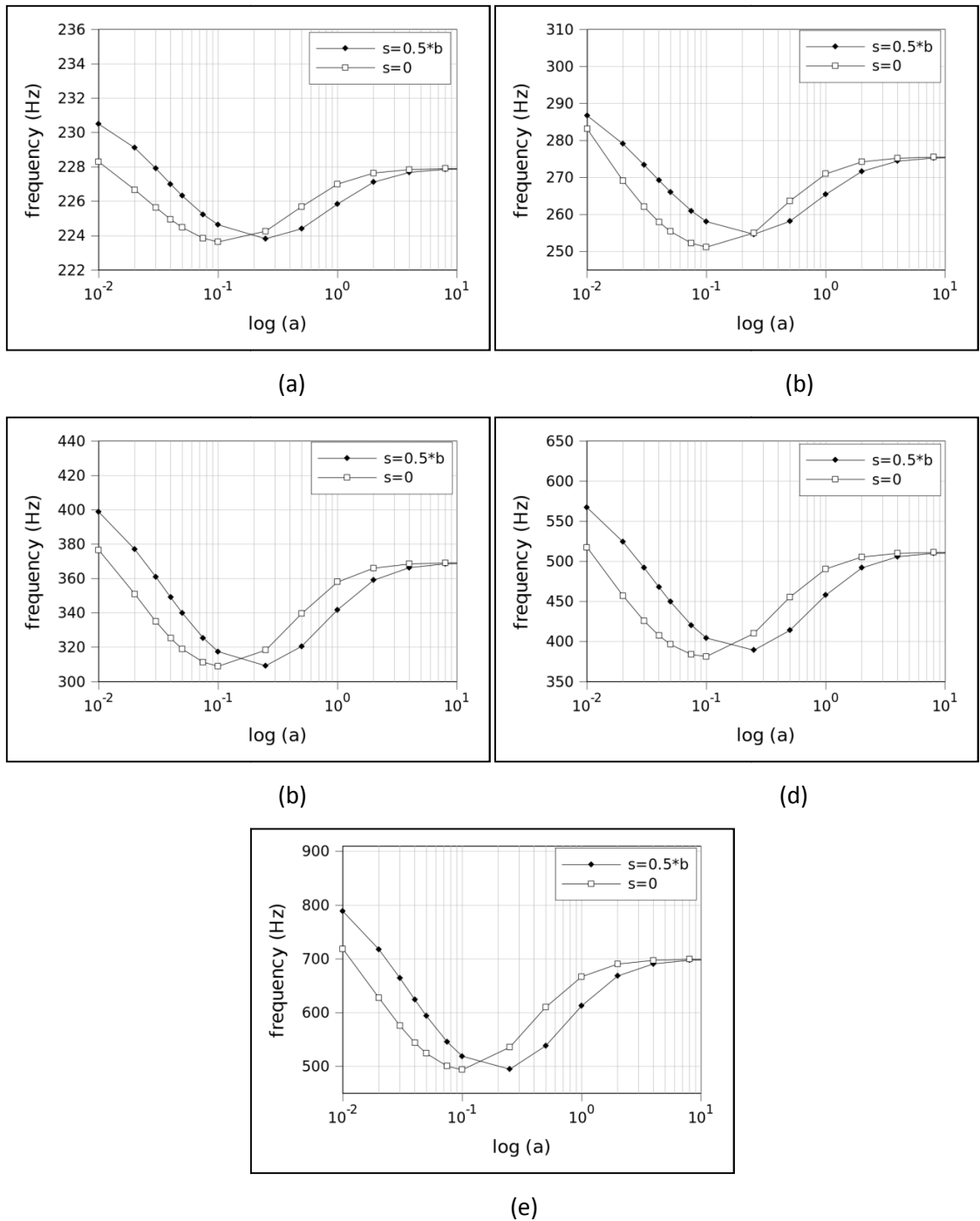
Figure 4.6. The frequency behavior of square plate with side lenght 0.3545 m and thickness 0.005 m as a function of tangential offset. Figures (a), (b), (c), (d), (e) shows the first, second, third, fourth, and fifth eigenvalues, respectively. These figures show a restricted area (x axis is restricted between 0.01 and 10 values) of the plots in Figure 4.5
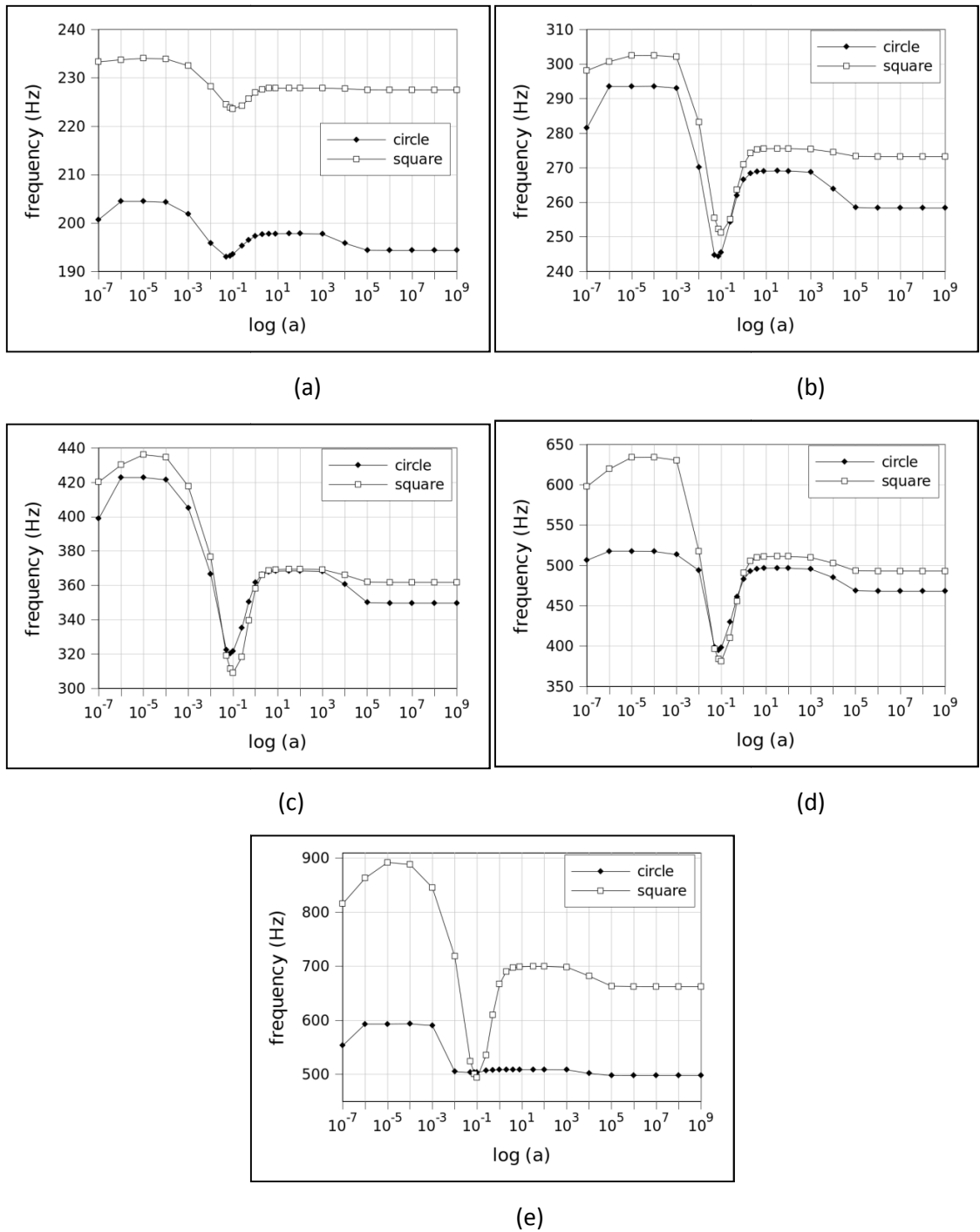
Figure 4.7. Effect of geometry on the frequency behavior of circle plate with radius 0.2 m and square plate with side lenght 0.3545 m are compared. Their areas are equal to each other, and thicknesses are both 0.005 m. Figures (a), (b), (c), (d), (e) shows the first, second, third, fourth, and fifth eigenvalues, respectively
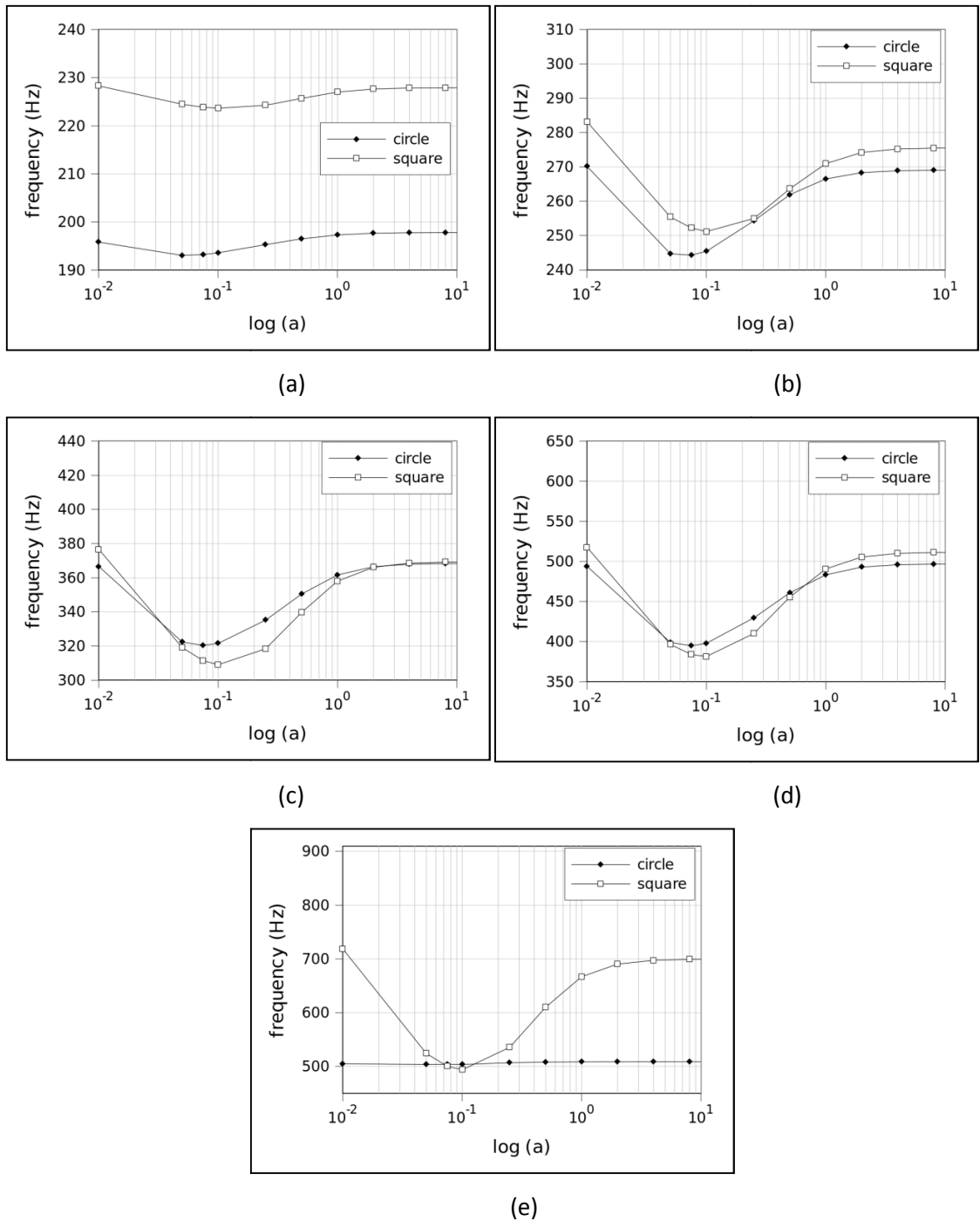
Figure 4.8. Effect of geometry on the frequency behavior of circle plate with radius 0.2 m and square plate with side lenght 0.3545 m are compared. Their areas are equal to each other, and thicknesses are both 0.005 m. Figures (a), (b), (c), (d), (e) shows the first, second, third, fourth, and fifth eigenvalues, respectively. These figures show a restricted area (x axis is restricted between 0.01 and 10 values) of the plots in Figure 4.7

Figure 4.9. Effect of wood type on the frequency behavior of square plate with side lenght 0.3545 m and thickness 0.005m. Figures (a), (b), (c), (d), (e) shows the first, second, third, fourth, and fifth eigenvalues, respectively

Figure 4.10. Effect of wood type on the frequency behavior of square plate with side lenght 0.3545 m and thickness 0.005m. Figures (a), (b), (c), (d), (e) shows the first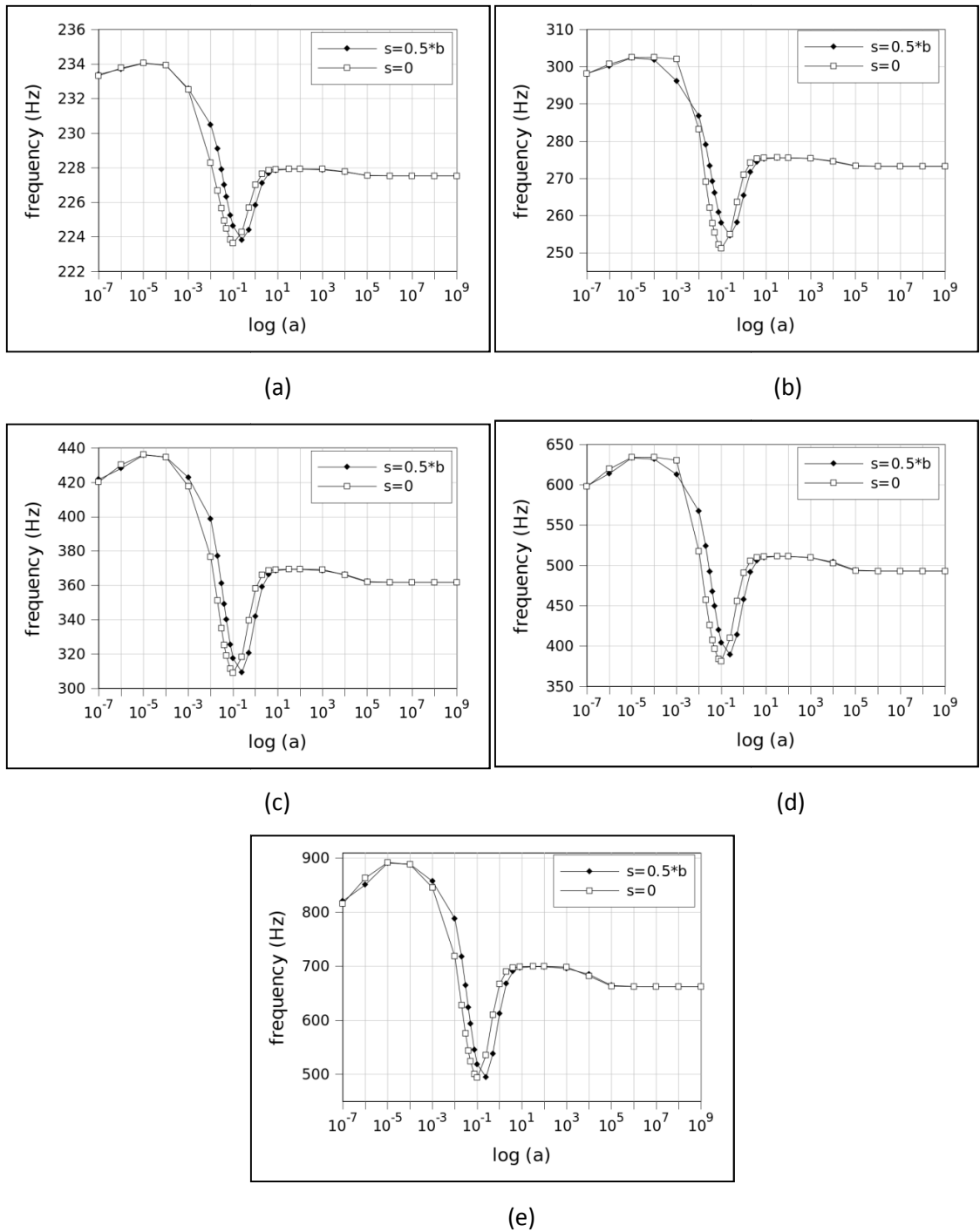, second, third, fourth, and fifth eigenvalues, respectively. These figures show a restricted area (x axis is restricted between 0.01 and 10 values) of the plots in Figure 4.9
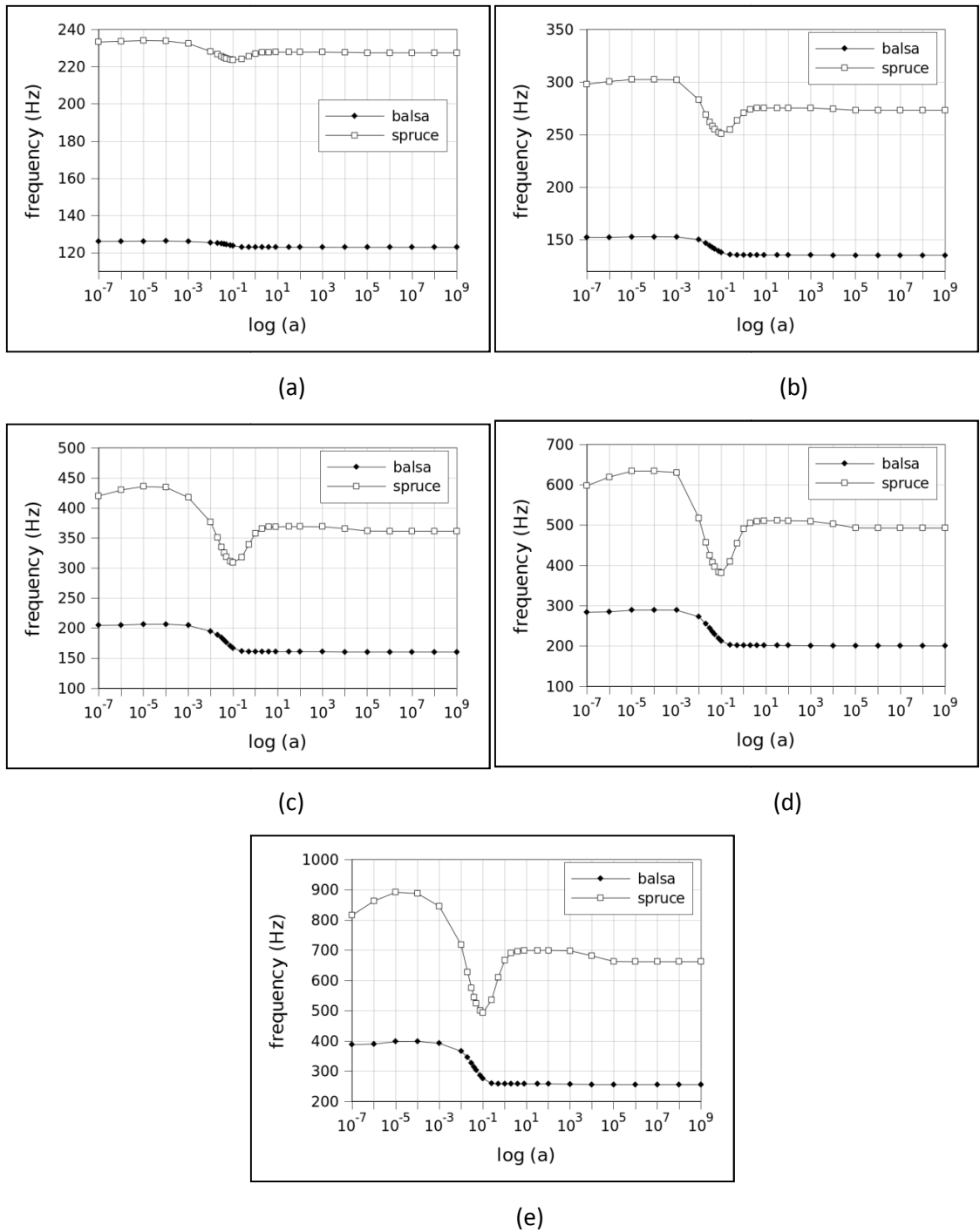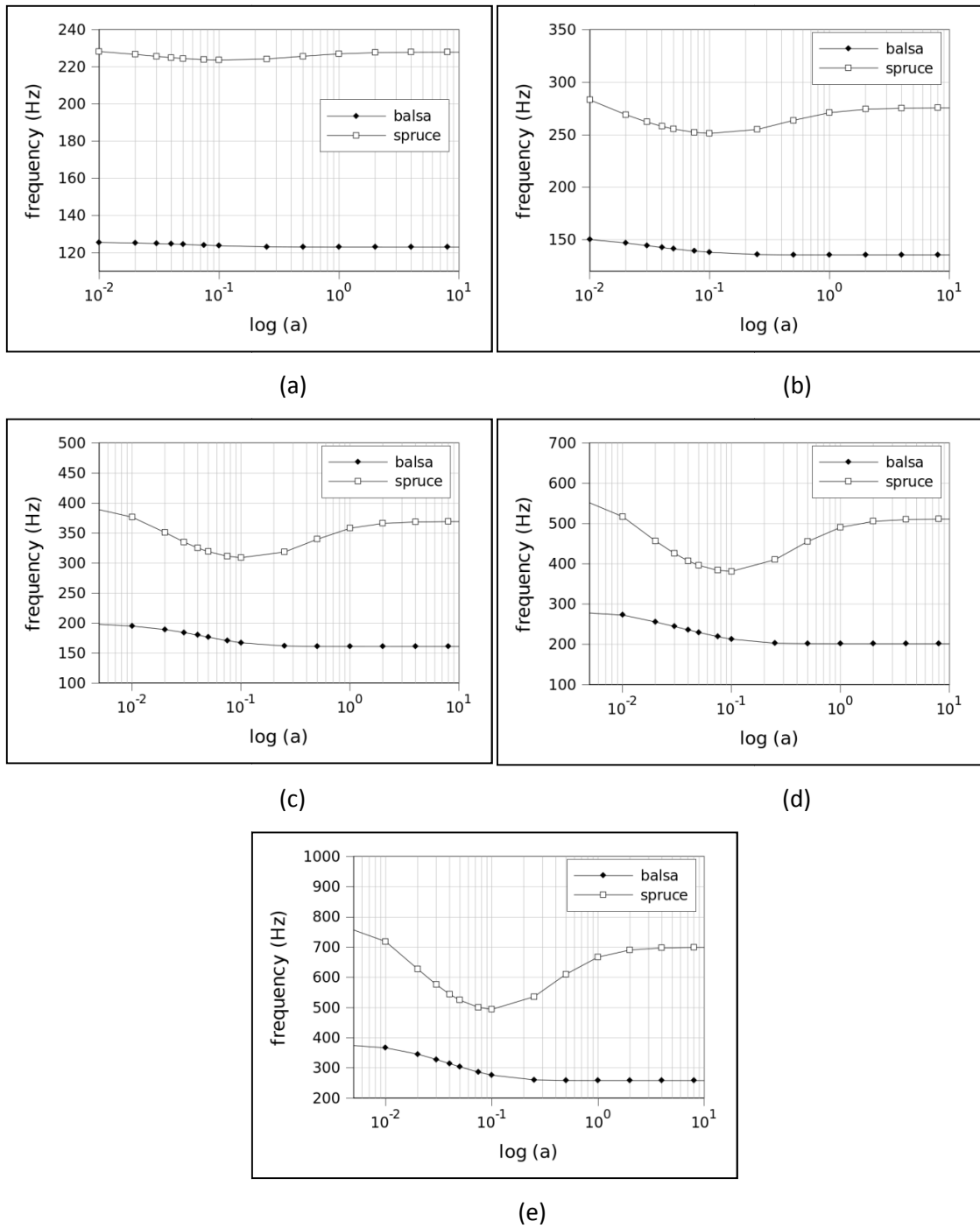
# 5. DISCUSSION

The numerical experimental results are given at the previous chapter for various types of cases. As stated before, the most important observation that we focus on is to understand the frequency behavior of axisymmetrically orthotropic material model with varying radial offset distance parameter. For this purpose, the numerous types of analyses are performed.

We begin by analyzing a clamped square plate to show the variation of frequency response at the limit values of the radial offset (first case is *a=0*, and the second case is *a* approaching infinity.) for first five eigenvalues as the initial work. Thus, the differences at the limit cases are shown clearly. After that, a number of numerical comparisons are done to compare the results obtained using the axisymmetrically orthotropic material model with the ones using the classical orthotropic material model. For that purpose, to validate the results of the finite element analyses Xing's study [1] is taken for the classical orthotropic case. Following these, the variation of eigenfrequencies is listed back to back with radial offset variation in an interval of $10^{-7}$ m and $10^{9}$ m. The frequency behavior of spruce sitka square plate is shown as a function of the radial offset and the tangential offset in Figure 4.4 and, Figure 4.5, respectively. Figure 4.6 is given for a selected portion of the radial offset value as zoomed view for the tangential offset variation case. Then, the geometry effect on the frequency behavior is examined using a square plate and a circular plate, and the related plots are given in Figure 4.7 and Figure 4.8. As the next analyses, the effect of wood type on the frequency behavior is studied using two types of wood: spruce sitka, and balsa. The orthotropic material properties of these woods are given at Appendix B. Similarly, the plots are given for the first five eigenvalues with varying radial offset value for the case that shows the effect of wood type in Figure 4.9 and Figure 4.10. Finally, the frequency behavior of spruce sitka square plate is shown as a function of shear presence in Figure 5.4. Now, the results are given for each of these cases mentioned above, respectively.

## 5.1. COMPARISON BETWEEN THE NUMERICAL SOLUTIONS OF THE CLASSICAL ORTHOTROPIC MATERIAL MODEL, AND THE LIMITING CASES OF AXISYMMETRIC ORTHOTROPIC MATERIAL MODEL

The plate of cut is made longitudinally such that its radial offset distance can be taken as equal to zero or approaching to infinity to perform the limiting case analyses. The theoratical explanation of these cases is examined as "limiting cases" at Section 2.1. As it is noted there, the dependence to the position information (i.e. "y" information) of the stiffness coefficients is removed as the radial offset approaches zero. In this case the effect of material properties along the tangential axis becomes immaterial. For this location, the cutting plane becomes a centroidal plane of symmetry which is parallel to the principal RL plane of orthotropy. In contrast, as the radial offset approaches infinity, i.e. the cutting plane is brought far away from the centroidal axis, the terms $\sin^2 \theta$ approaches zero and the radial properties dissepear. Here, it becomes parallel to the principal TL plane of orthotropy. The related drawing is given in Figure 5.1 below. For these two distinct cases, plates local coordinate system gets rotated 90 degrees about the longitudinal axis, from the radial direction of orthotropy for the case which radial offset equals to zero, to the tangential direction for the case radial offset approaches infinity.

Table 5.1 indicates the variation of frequency response with radial offset of clamped square plate made from spruce sitka for radial offset approaching infinity, and zero cases. $\omega_i^{TL}$ corresponds to the ith natural frequency of a plate that lies along the TL plane while $\omega_i^{RL}$ is that of a plate lying along the RL plane; both of which are derived from the classical orthotrpic plate solution. It is observed that as radial offset is brought to infinity the solution of the axisymmetrical orthotropic material model converges to that of a plate lying in the TL plane predicted by the clasically orthotropic material model. Vice versa, as radial offset becomes zero, the solution of the former solution converges to that of a plate lying in the RL plane predicted by the latter solution. It is worth noting that the values from each solution are same to four significant digits.
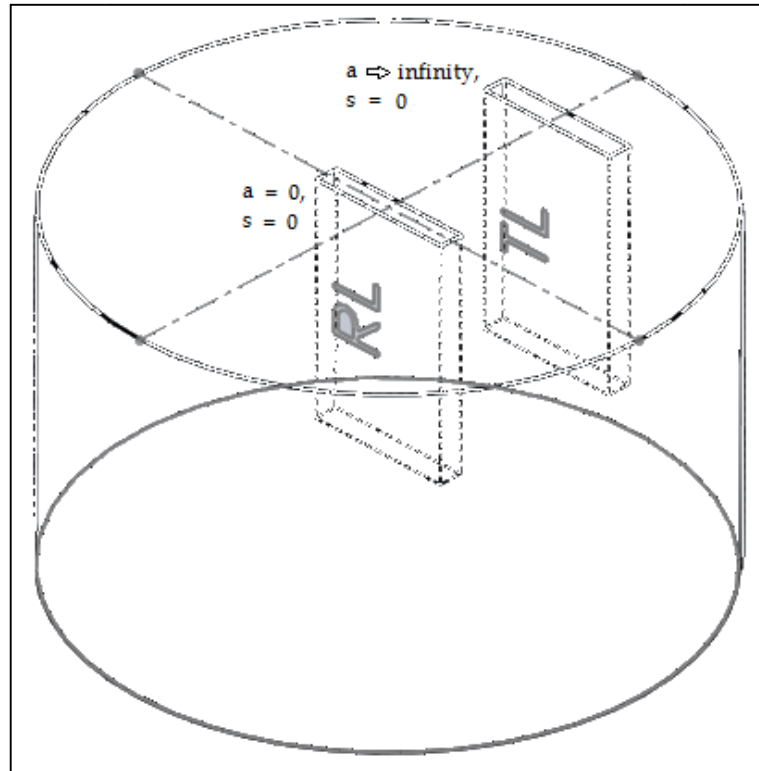
Figure 5.1. The cutting plane described as a function of radial offset, $a$, from the centroidal axis. Location of the cutting plane leads to a singular orthotropic orientation at $a=0$. For this location, the cutting plane becomes parallel with the RL plane. As radial offset is taken to infinity it becomes parallel to the TL plane

Table 5.1. Verification of frequency response with radial offset of clamped square plate made from spruce sitka for approaching to infinity, and zero cases

|  | $\omega_i^{TL}$ | $\lim\limits_{a \to \infty} \omega_i(a)$ | $\omega_i^{RL}$ | $\omega_i(0)$ |
|---|---|---|---|---|
| $\lambda_1$ | 227.54 | 227.54 | 233.31 | 233.31 |
| $\lambda_2$ | 273.28 | 273.28 | 297.55 | 297.55 |
| $\lambda_3$ | 361.82 | 361.82 | 419.45 | 419.46 |
| $\lambda_4$ | 493.26 | 493.26 | 593.58 | 593.59 |
| $\lambda_5$ | 662.71 | 662.71 | 810.56 | 810.57 |

## 5.2. VALIDATION OF AXISYMMETRICALLY ORTHOTROPIC MATERIAL MODEL RESULTS WITH THOSE OF AN ANALYTICAL SOLUTION

To validate the axisymmetrically orthotropic material model results with an analytical solution, Xing's study [1] is used as the analytical solution. At this study, the eigenvalue equations are solved using Newton's method, and a dimensionless frequency parameter $= b\sqrt[4]{\omega^2 \rho h / F_1}$ , where $b$ is the shorter side length of the rectangle, $\omega$ is the corresponding eigenvalue, $\rho$ is the mass density, $h$ is the thickness, and $F_1$ is the bending stiffness parameter, is defined in order to be used at the analyses. The geometry of problem is shown in Figure 5.2.
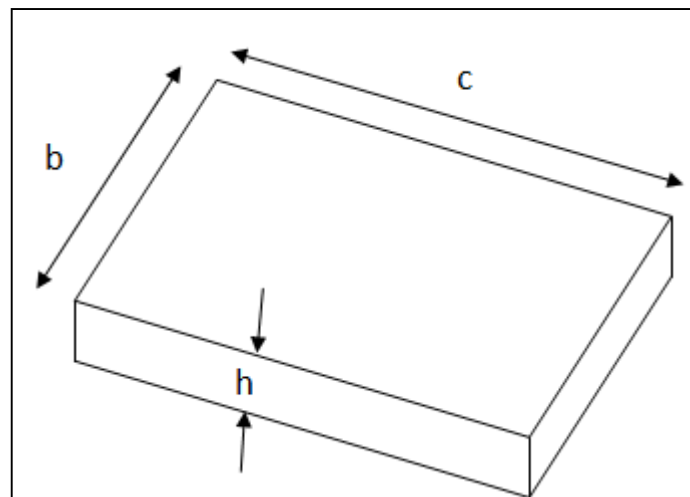


Figure 5.2. A rectangle plate and its dimensions

At the same study, this frequency parameter is calculated using different types of material for different geometrical configurations of a rectangle plate. Only the clamped boundary condition solutions are compared with our study. Material list for four different composites types used at the analysis are given at Table 5.2.

Table 5.2. Type of the material properties

| No | Material | $E_L$ (GPa) | $E_T$ (GPa) | $G_{LT}$ (GPa) | $v_{LT}$ | $\rho$(kg/m) |
|----|----------|-------------|-------------|----------------|----------|--------------|
| 1 | T-graphite / epoxy | 185 | 10.5 | 7.3 | 0.28 | 1600 |
| 2 | B-boron / epoxy | 208 | 18.9 | 5.7 | 0.23 | 2000 |
| 3 | K-arly / epoxy | 76 | 5.6 | 2.3 | 0.34 | 1460 |

Table 5.3 shows the variation of frequency parameter $\gamma = b\sqrt[4]{\omega^2 \rho h / F_1}$ for the clamped square plate with side length 1 m and material type 2. Axisymmetrically orthotropic material model analyses for this case are done for three different mesh densities. Xing's [1] results are compared with axisymmetrically orthotropic material model solution, and the errors in percentage values are noted right next to the axisymmetrically orthotropic material model values in parathesis. Standart axisymmetrically orthotropic material model mesh density is 100 by 100. AOMM[#] indicates 200 by 200 meshing while AOMM[*] analyses are evaluated using the 220 by 220 meshing. A sample meshing plot is given in Figure 5.3 below.



Figure 5.3. Clamped square mesh types showing the boundary conditions in red colour.
Figure indicates 100 by 100 meshing

For our study, the errors about 0.5 % are acceptable and nearly all results given at the Table 5.3 are below that number.

Table 5.3. Frequency parameter for clamped square plate with side length 1 m and Material 2

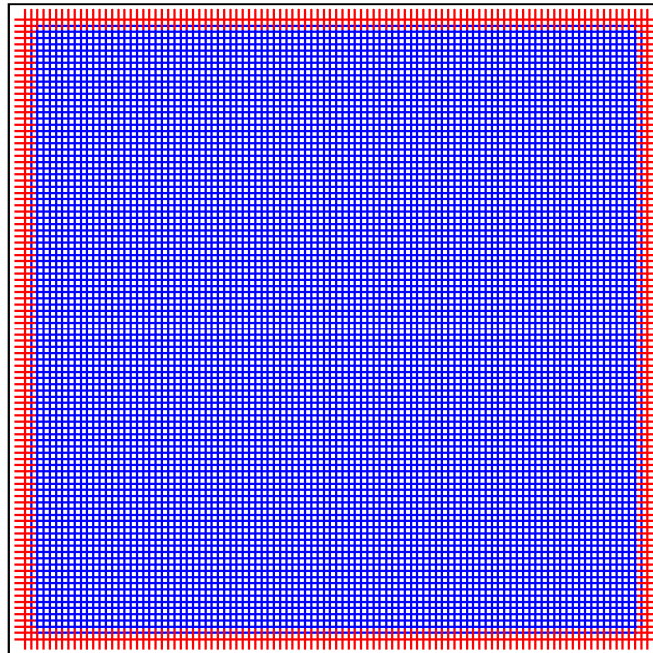| c (m) | b (m) | Method | Frequecncy parameter of for first five eigenvalues and errors in percentage | | | | |
|---|---|---|---|---|---|---|---|
| | | | $\lambda_1$ | $\lambda_2$ | $\lambda_3$ | $\lambda_4$ | $\lambda_5$ |
| 1.0 | 1.0 | Xing | 4.87 | 5.50 | 6.68 | 7.91 | 8.15 |
| | | AOMM | 4.88 (0.21) | 5.52 (0.36) | 6.70 (0.30) | 8.17 (3.29) | 9.76 (19.7) |
| | | AOMM$^{\#}$ | same | same | same | 8.16 (3.16) | 8.16 (0.12) |
| | | AOMM$^{*}$ | same | same | same | 7.92 (0.13) | 8.17 (0.24) |

Another important observation about the Table 5.3 is the error difference at the fourth and fifth eigenvalues of three different meshed analyses. Generally, finite element analyses are affected by mesh density, and for less denser meshes some eigenvalues may be missing especially at the higher sequence numbers of eigenvalues. When the 100 by 100 mesh results are examined it is seen that there is nonignorable error between Xing's solution and axisymmetrically orthotropic material model solution for the fourth and fifth eigenvalues. Then, when the 200 by 200 meshing is examined, the fifth eigenvalue matches with the Xing's solution but the fourth eigenvalue is seemed to be still missing by the axisymmetrically orthotropic material model solution. As the final run, 220 by 220 meshing is applied for the same geometry, and for all five eigenvalues there is a perfect match between the frequency parameter results of Xing's solutions and axisymmetrically orthotropic material model ones. Thus, depending on the application type and how sensitivity results the user would like to obtain, the mesh density should be increased for the finite element analysis.

Table 5.4 shows the variation of frequency parameter $\gamma = b\sqrt[4]{\omega^2 \rho h / F_1}$ for clamped plates with variable b for all the material types. For this analyses mesh density is taken as 100 by 100 as standart. Xing's results are compared with axisymmetrically orthotropic

material model solution, and the errors in percentage values are noted right next to the axisymmetrically orthotropic material model values in paranthesis. It can be be seen on the table that the maximum error between Xing's solution and axisymmetrically orthotropic material model is 0.53 % for material 1 which is in acceptable region for us. For the other two geometrical combinations, i.e. c x b = 1m x 2m and c x b = 1m x 2m, like the previous one, axisymmetrically orthotropic material model solutions are again satisfying when compared with the Xing's solutions. Thus, this completes the validation of axisymmetrically orthotropic material model results with the ones in the literature, i.e. Xing's solutions.

Table 5.4. Frequency parameter for clamped plates with variable b and Material 3

| c (m) | b (m) | Method (Material No) | Frequecncy parameter of for first five eigenvalues and errors in percentage | | | | |
|---|---|---|---|---|---|---|---|
| | | | $\lambda_1$ | $\lambda_2$ | $\lambda_3$ | $\lambda_4$ | $\lambda_5$ |
| 1.0 | 1.2 | Xing (M1) | 4.80 | 5.08 | 5.68 | 6.56 | 7.60 |
| | | AOMM(M1) | 4.81 (0.21) | 5.10 (0.39) | 5.71 (0.53) | 6.58 (0.30) | 7.62 (0.26) |
| 1.0 | 2.0 | Xing (M2) | 4.75 | 4.82 | 5.00 | 5.32 | 5.78 |
| | | AOMM(M2) | 4.75 (-) | 4.83 (0.21) | 5.01 (0.20) | 5.33 (0.19) | 5.80 (0.35) |
| | | Xing (M3) | 4.75 | 4.82 | 4.98 | 5.26 | 5.68 |
| | | AOMM(M3) | 4.75 (-) | 4.82 (-) | 4.99 (0.20) | 5.28 (0.38) | 5.69 (0.18) |
| 1.0 | 3.0 | Xing (M2) | 4.74 | 4.76 | 4.81 | 4.90 | 5.05 |
| | | AOMM(M2) | 4.74 (-) | 4.74 (-) | 4.81 (-) | 4.91 (0.20) | 5.06 (0.19) |
| | | Xing (M3) | 4.74 | 4.76 | 4.81 | 4.90 | 5.03 |
| | | AOMM(M3) | 4.74 (-) | 4.76 (-) | 4.81 (-) | 4.90 (-) | 5.04 (0.19) |

## 5.3. COMMENTS ON THE EFFECT OF RADIAL OFFSET AND TANGENTIAL OFFSET ON THE FREQUENCY BEHAVIOR

The analyses examining the effect of the radial offset show like a V-shaped curve behavior for the values between 0.01 m and 1 m as given in Figure 4.4. This may be the most important observation for our study since it seems like there is a critical radial offset distance value (for this case it is 0.1 m) which the frequencies show minimum value. At

that point, the frequency values also show nearly a symmetrical behavior at the right and left sides of this minimum value.

On the other hand, the frequency values show characteristic behavior at the limit cases of radial offset distance values for all five cases of analyses. Mathematically, as the radial offset distance goes to an infinite value it is expected that the values show asymptotic behavior. Therefore, it is seemed that the curve fits to a constant value of frequency asymptotically after a certain value which is $10^5$ m for this case of interest. From the definition of limit, for radial offset distance values approaching to zero, the curve should have a zero tangent region for derivative continuity at zero value for even functions. Since the function in our study is defined as $(y/a)^2$ where $y$ is the actual position coordinate of corresponding mesh element, we have an even function so that it is expected from curve to reach a minimum value at zero radial offset value. So, the tendency of decrease starting from $10^{-5}$ m indicates that it will reach to a minimum value and shows zero tangent behavior.

Figure 4.5 and Figure 4.6 indicate the effect of tangential offset with varying radial offset distance. At all plots given in Figure 4.6, it is obviously seemed that the frequency values for *s = 0.5 x b m* are higher than the ones for *s = 0* up to a definite value which is about 0.2 m for this case of interest. After that point, the frequency values of *s = 0* case becomes higher than the other one. So, there is clearly a turning point for these plots listed in Figure 4.6. The V-shaped behavior shows almost linearly increasing and almost linearly decreasing behavior at the right and left sides of this turning point. Like the previous case of radial offset distances varying case, the curve clearly shows zero tangent behavior for the very small values of tangential offset distance values, and asymptotic behavior at the values of radial offset distance approaching to infinity.

## 5.4.  COMMENTS ON THE EFFECT OF GEOMETRY ON THE FREQUENCY BEHAVIOR

Figure 4.7 and Figure 4.8 the variation of the frequency values with changing the radial offset distance for a clamped square plate and a clamped circle plate with radius. The most important observation about these results is that the frequency value of analyses

performed with square geometry is always higher than the ones with circle geometry for all first five eigenvalues. The general behavior of the curves of both geometries is similar with the previous analyses. Again, the zero tangent portion, asymptotic region, and the V-shaped areas are clearly being seen on all plots of Figure 4.7 andFigure 4.8. However, for the fifth eigenvalue, the behavior of circle geometry solution seems to be much more different that the previous ones. This is not an exceptional solution case; actually this is an example of numerical error case. As mentioned before at the rectangular geometry solution cases using axisymmetrically orthotropic material model, there may be these kinds of numerical errors when the mesh density is lower than a certain value. So, in this case, if someone would like to obtain more accurate results for the frequency values of the fifth eigenvalue, he/she should increase the mesh size. The weird behavior of the fifth eigenvalue caused by the numerical error can be seen much more clearly in Figure 4.8e.

Another important observation about the plots in Figure 4.7 is that there is a sharp linearly decreasein portion of values between the values $10^3$ m and $10^5$ m. After the ending point of this line, the asymptotic behaviour begins to be observed clearly. The turning point of the curves (i.e. the frequency values of circle geometry is higher than the ones of square geometry up to a point. After that point the behavior changes oppositely and the frequency values of square geometry are getting higher than the other ones.) are again observed clearly.

## 5.5. COMMENTS ON THE EFFECT OF WOOD TYPE ON THE FREQUENCY BEHAVIOR

There is an obvious observation about the results which examine the effect of wood types on the frequency behavior: The values of frequencies using a spruce sitka case is almost doubled the values of balsa at each of the five runs. These are listed in Figure 4.9 and Figure 4.10. This is an expected result because of their different orthotropic material behaviors. Balsa is lighter material than the spruce sitka, so spruce sitka is said to be stiffer material than balsa. This is why the frequency values of analyses using spruce sitka is always higher than the ones obtained with using balsa wood. As it can be seen on the zoomed plots, balsa wood behaves similarly to spruce sitka up to a minimum point of

frequency values at all cases of eigenvalues. However, after that point, balsa does not behave like spruce sitka and it is rapidly starting the asymptotic behavior.

One of the most important outcomes of these analyses is that the curve behavior of the spruce sitka and balsa woods are different than each other. Spruce sitka curve behaves like our previous analyses but the balsa curve does not have a V-shaped region like spruce sitka.

## 5.6. EFFECT OF SHEAR PRESENCE ON THE FREQUENCY BEHAVIOR

In Figure 5.4, the frequency behavior of spruce sitka clamped square plate with side length 0.3545 m and thickness 0.005 m is examined as a function of shear presence with the varying radial offset distance value. Two cases of shear presence are examined here: one is the no shear case, while the other is the case that the shear factor (kappa) is 5/6 which is the default value of the finite element solver.

The analyses indicate that the frequency values with including shear cases are always lesser than the ones obtained with no shear case.

The zero tangent region of the analyses of no shear are wider than the other case. Also the no shear case fits to an asymptotic line sooner than including shear case. As a general observation, the effect of shear presence on the frequency behavior plays an important role on the limit cases although the difference between the values of frequency between these two analyses is low (for example, this difference is only about 2 Hz., and 10 Hz for $a=10^{-7}$ m value at the first eigenvalue and second eigenvalue analyses, respectively.).
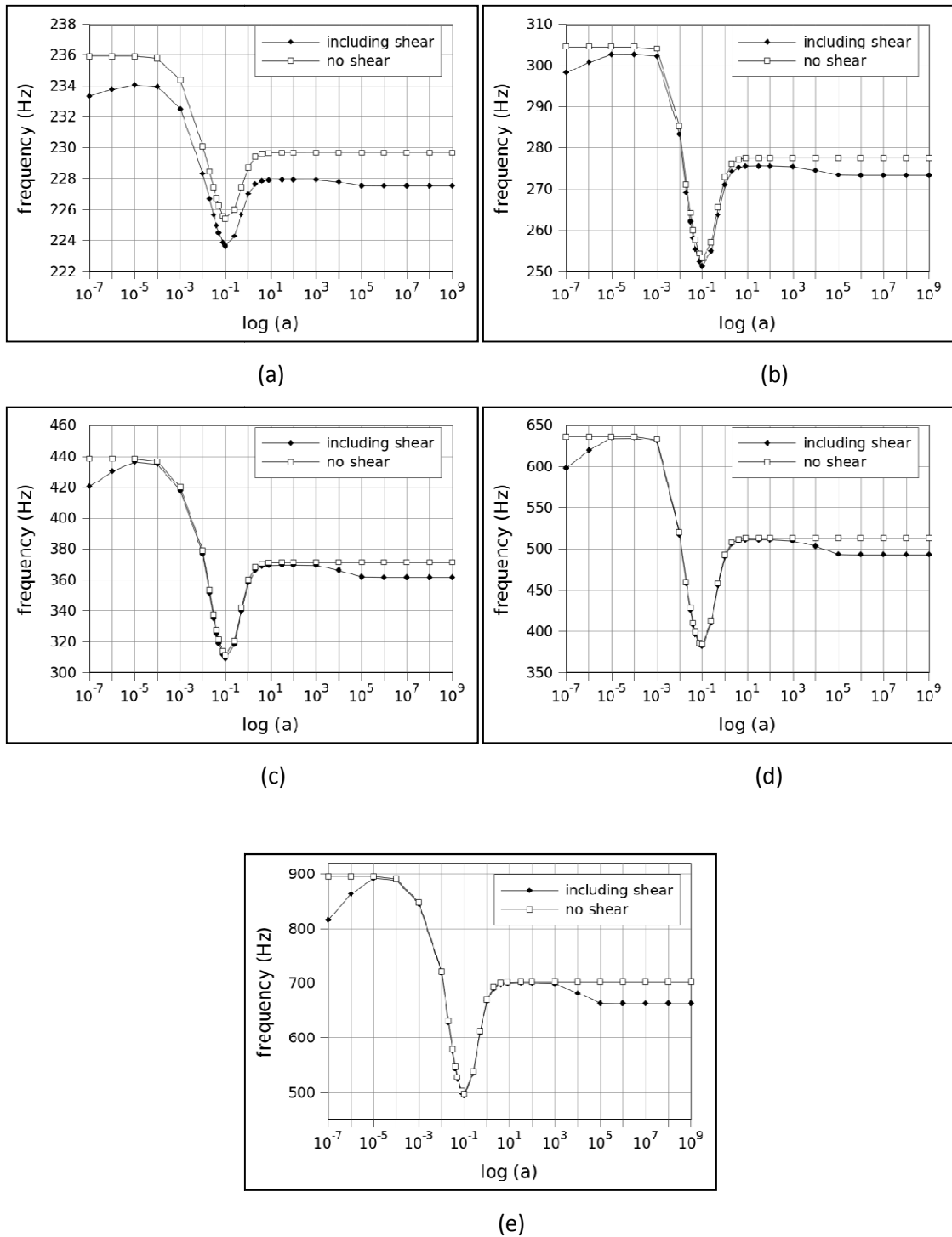
Figure 5.4. The frequency behavior of spruce sitka square plate with side lenght 0.3545 m and thickness 0.005 m as a function of shear presence. Figures (a), (b), (c), (d), and (e) shows the first, second, third, fourth, and fifth eigenvalues, respectively

# 6. CONCLUSION AND FUTURE WORKS

In this study, a new finite element material model is developed with concise formulation that takes into account the variation in the alignment of the principal axes of orthotropy in order to examine the frequency behavior of the longitudinally cut thick plates. More different than the existing studies that use classical orthotropic material model, the components of the stiffness matrix are updated pointwise along the surface of plate as a result of the varying orthotropic orientation angle.

Wood is selected as the axisymmetrically orthotropic material, and a number of analyses are performed. Basically, the results are focused to indicate the effects of variation of the radial offset parameter on the frequecny behavior. Apart from that, a couple of discussions are given for different kinds of analyses such as the analyses showing the effect of geometry, wood type, and the shear presence.

This study completes the formation of the stiffness matrix of an axisymmetricaly orthotropic material model, and someone can perform a finite element analysis of longitudinally cut thick plates using this new model and using the finite element solver, FEAP, with its new subroutines which are developed in this study. In addition, a couple of future works would be applied in the light of this study. For instance, a shape optimization project may be executed in order to develop an acoustically perfect shaped musical instrument. Since the frequency values of each syllables at resonant are well-known, an optimum plate shape, which gives its mode shapes exactly at these resonant values, can be obtained for any type of wood. As another example of the possible future works is to make an application of variable thickness analyses in order to be used for any selected application.

# APPENDIX A: MATERIAL SUBROUTINE

Updated material subroutine is defined as the name of *umatpl* at the program. The reduced form of the stiffness matrix for the normal and shear stresses is defined as *dmg* matrix, and the reduced stiffness matrix that includes the shear terms is defined as *dsg* matrix. The whole subroutine is given below.

```
c$Id:$
      subroutine umatpl(d,psi,dmg,dsg)


c     Rotation of material arrays from principal to local element
directions



c     Inputs: d         - Array with material properties
c             psi       - Angle from y1-axis (local) to 1-axis
(principal)
c     Output: dmg(3,3) - Plane stress modulus matrix
c             dsg(2,2) - Transverse shear modulus matrix



c-----[--.----+----.----+----.-----------------------------------
-----]

      implicit  none

      integer   i, j

      real*8    psi, si, co, s2, c2, s4, s8, c4, c8, cs
      real*8    E1, E2, E3, v12, v23, v31, v21, v13, v32
      real*8    g12, g23, g31, R

      real*8    d(*)
```

```
      real*8    dml(3,3), dmg(3,3), dsg(2,2), qm(3,3), dmlqj(3)

      save

c     Set up constants for transformation

      si = sin(psi)
      co = cos(psi)
      s2 = si*si
      s4 = s2*s2
      s8 = s4*s4
      c2 = co*co
      c4 = c2*c2
      c8 = c4*c4
      cs = co*si
      E1 = d(231)
      E2 = d(232)
      E3 = d(233)
      v12 = d(234)
      v23 = d(235)
      v31 = d(236)
      v21 = (E2/E1)*v12
      v13 = (E1/E3)*v31
      v32 = (E3/E2)*v23
      g12 = d(237)
      g23 = d(238)
      g31 = d(239)
      R = (1/E2)*(1-v21*v12)*c4+(1/E3)*(1-v31*v13)*s4
     &  +(1/g23-v23/E2-v32/E3-2*v12*v13/E1)*c2*s2

c     Convert plane stress local to global matrix

      dmg(1,1) = E1*((c4/E2)+(s4/E3)+(1/g23-v23/E2-
    v32/E3)*c2*s2)/R
```

```
      dmg(1,2) = (v12*c2+v13*s2)/R

      dmg(1,3) = 0

      dmg(2,1) = dmg(1,2)

      dmg(2,2) = 1/R

      dmg(2,3) = 0

      dmg(3,1) = 0

      dmg(3,2) = 0

      dmg(3,3) = 1/(c2/g12+s2/g31)


c     Set up global shear matrix

      dsg(2,2) = d(37)*(g23*c4+g23*s4+s2*c2*((E3/R)
     &          *(1-v12*v21-v21*v13-v23)+(E2/R)
     &          *(1-v12*v31-v13*v31-v32)-2*g23))

      dsg(1,1) = d(37)*(g31*c2+g12*s2)

      dsg(1,2) = 0

      dsg(2,1) = 0


      end
```

## APPENDIX B: MATERIAL PROPERTIES OF WOODS

The orthotropic material properties of spruce sitka and balsa woods are given at the below table:

| | $E_L$ (N/m$^2$) | $E_T$ (N/m$^2$) | $E_R$ (N/m$^2$) | $\nu_{LT}$ | $\nu_{TR}$ | $\nu_{RL}$ | $G_{LT}$ (N/m$^2$) | $G_{TR}$ (N/m$^2$) | $G_{RL}$ (N/m$^2$) |
|---|---|---|---|---|---|---|---|---|---|
| Spruce Sitka | $108.2*10^8$ | $4.7*10^8$ | $8.4*10^8$ | 0.47 | 0.24 | 0.04 | $66*10^8$ | $3*10^8$ | $69*10^8$ |
| Balsa | $33.8*10^8$ | $0.5*10^8$ | $1.6*10^8$ | 0.49 | 0.23 | 0.02 | $12*10^8$ | $2*10^8$ | $18*10^8$ |

# REFERENCES

1. Xing Y. F. and Liu B., "New exact solutions for free vibrations of thin orthotropic rectangular plates", *Compos Struct,* vol. 89, pp. 567–574, 2009.

2. Hearmon R. F. S., The fundamental frequency of vibration of rectangular wood and plywood plates, *Proc. Phys. Soc.*, vol. 58, n.78, pp. 78-92, 1946.

3. Timoshenko S., "The theory of plates and shells", *New York: McGraw-Hill*, 1940.

4. Leissa A. W., "Vibration of Plates", *NASA SP-160*, 1969.

5. Leissa A. W., "The free vibrations of rectangular plates", *J Sound Vib*, vol. 31, n. 3, pp. 257-293, 1973.

6. Hearmon R. F. S., "The frequency of flexural vibration of rectangular orthotropic plates with clamped or supported edges", *Journal of Applied Mechanics*, vol. 26, pp. 537-540, 1959.

7. Warburton G. B., "The vibration of rectangular plates", *Proceedings of the Institution of the Mechanical Engineers*, vol.168, pp. 371-384, 1954.

8. Jones R., Milne B. J., "Application of the extended Kantorovich method to the vibration of clamped rectangular plates", *J Sound Vib*, vol. 45, n. 3, pp. 309-316, 1976.

9. Bhat R. B., "Natural frequencies of rectangular plates using characteristic orthogonal polynomials in Rayleigh-Ritz method", *J Sound Vib*, vol. 102, n. 4, pp. 493-499, 1985.

10. Sakata T., Takahashi K., Bhat R. B., "Natural frequencies of orthotropic rectangular plates obtained by iterative reduction of the partial differential equation", *J Sound Vib*, vol. 189, n. 1, pp. 89-101, 1996.

11. Kim S. C., "Natural frequencies of orthotropic, elliptical and circular plates", *Journal of Sound and Vibration* vol. 259, n. 3, pp. 733–745, 2003.

12. Biancolini M. E., Brutti C. and Reccia L., "Approximate solution for free vibrations of thin orthotropic rectangular plates", *J Sound Vib,* vol. 288, pp. 321–344, 2005.

13. Rossi R. E., Bambill D. V. and Laura P. A. A., "Vibrations of a rectangular orthotropic plate with a free edge: comparison of analytical and numerical results", *Ocean Engineering,* vol. 25, n. 7, pp. 521–527, 1998.

14. Sakata T., "Natural frequencies of clamped orthotropic rectangular plates with varying thickness", *Journal of Applied Mechanics*, vol. 45, pp. 871-876, 1978.

15. Cheung, Y. K., and Zhou, D., "The Free Vibrations of Tapered Rectangular Plates Using a New Set of Beam Functions with the Rayleigh-Ritz Method", *J Sound Vib*, vol. 223, n. 5, pp. 703-722, 1999.

16. Grigorenko A. Ya. and Tregubenko T. V., "Numerical and experimental analysis of natural vibrations of rectangular plates with variable thickness", *International Applied Mechanics*, vol. 36, n. 2, pp. 268-270, 2000.

17. Huang M., Ma X. Q., Sakiyama T., Matuda H., Morita C., "Free vibration analysis of orthotropic rectangular plates with variable thickness and general boundary conditions", *J Sound Vib,* vol. 288, pp. 931–955, 2005.

18. Dian-Yun Chen and Bao-Sheng Ren, "Finite element analsis of the lateral vibrations of thin annular and circular plates with variable thickness", *Journal of Vibration and Acoustics*, vol. 120, pp. 747-752, 1998.

19. Chakraverty S., Ragini Jindal, Agarwal V. K., "Vibration of nonhomogeneous orthotropic elliptic and circular plates with variable thickness", *Journal of Vibration and Acoustics*, vol. 129, pp. 256-259, 2007.

20. Goodman James R., ASCE M., Bodig J., "Orthotropic elastic properties of wood", *Journal of Structural Division, Proc. of the American Society of Civil Engineers*, vol. 96, n. 10, pp. 2301-2319, 1970.

21. Mascia N. T., Lahr. F. A. R., "Remarks on orthotropic elastic models applied to wood", *Materials Research*, vol. 9, n. 3, pp. 301-310, 2006.

22. Noack D., Roth W., "On the theory of elasticity of the orthotropic material wood", *Wood Science and Technology*, vol. 10, pp. 97-110, 1976.

23. Lawrence J. Katz, Paulette Spencer, Yong Wang, Anil Misra, Orestes Marangos and Lisa Friis, "On the anisotropic elastic properties of woods", *J Mater Sci*, vol. 43, pp. 139-145, 2008.

24. Jones Robert M., "Mechanics of Composite Materials", *Hemisphere Publishing Corporation*, 1975.

25. Richard M. Christensen, "Mechanics of Composite Materials", *Dover Publications*, 2005.

26. Lekhnitskii S. G., "Anisotropic plates, translated by S. W. Tsai and T. Cheron", *New York: Gordon and Breach Science Publishers*, 1967.

27. Dassault Systems, Solidworks. URL: *http://help.solidworks.com/2010/English/SolidWorks/cosmosxpresshelp/AllContent/SolidWorks/NonCore/SimulationXpress/c_Orthotropic_Material.html?id=be34fd51a07d45c28872d994138dbb77#Pg0*

28. Reiterer A., Sinn G., Stanzl-Tschegg S. E.*,* "Fracture characteristics of different wood species under mode I loading perpendicular to the grain"*, Mat. Sci. Eng. A-Struct., vol.* 332, pp. 29-36, 2002.

29. Gibson L. J., Ashby M. F., "Cellular Solids: Structure and Properties"*, Pergamon Press,* 1988.

30. Beery W. H., Ifju G., McLain E., "Quantitative wood anatomy –relating anatomy to transverse tensile strength". *Wood Fiber Sci.* vol. 15, pp. 395–407, 1983.

31. Thuvander F., Berglund L. A., "In situ observations of fracture mechanisms for radial cracks in wood"*, J.Mater. Sci.,* vol. 35, pp. 6277-6283, 2000.

32. Mishnaevsky L., Qing H.*,* "Micromechanics of wood: state-of-the-art review", *Research Report Computational Mesomechnics of Composites, Technical University of Denmark,* 2008.

33. Cıblak Namık, Personal correspondance for his unpublished manuscript.

34. Reddy J. N., "Energy Principles and Variational Methods In Applied Mechanics", *John Wiley and Sons, Inc.*, Second Edition, 2002.

35. Graham S. Kelly, "Fundamentals of Mechanical Vibrations", *McGraw-Hill*, Second Edition, 2000.

36. Reddy J. N., "Theory and Analysis of Elastic Plates", *Taylor and Francis*, 1999.

37. McLachlan N., "Bessel Functions for Engineers", *Oxford University Press*, 1948.

38. Vernet D., "Influence of the guitar bracing using Finite element method"*, Technical Report The University of New South Wales and Ecole Normale Superiore,* 2001.

39. University of New South Wales, URL:

    *http://www.phys.unsw.edu.au/~jw/guitar/patterns_engl.html*

40. Reissner E., "The effect of transverse shear deformation on the bending of elastic plates", *J. Appl. Mech.*, vol. 12, pp.69-76, 1945.

41. Mindlin R. D., "Influence of rotatory inertia and shear in flexural motions of isotropic elastic plates", *J. Appl. Mech.*, vol. 18, pp.31-38, 1951.

42. Zienkiewicz O. C., Taylor R. L., "The Finite Element Method for Solid and Structural Mechanics", *Butterworth-Heinemann*, Sixth Edition, 2005.

43. Taylor Robert L., "FEAP User Manual", 2008.